

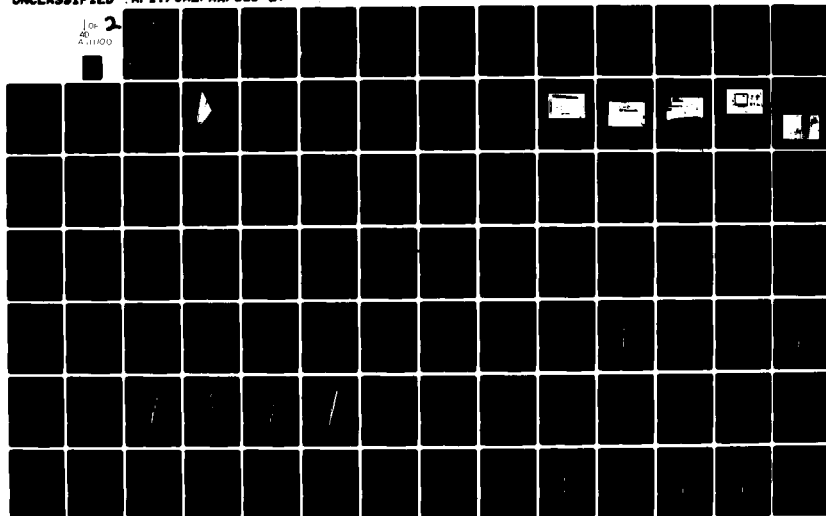
AD-A111 100

AIR FORCE INST OF TECH WRIGHT-PATTERSON AFB OH SCHOO--ETC F/S 1/1
INVESTIGATION OF A TWO-DIMENSIONAL MODEL FOR THE PREDICTION OF --ETC(U)
DEC 81 J O SANDY
AFIT/GAE/AA/81D-27

UNCLASSIFIED

NL

1 of 2
AD-A111100



ADDITION

LEVEL II

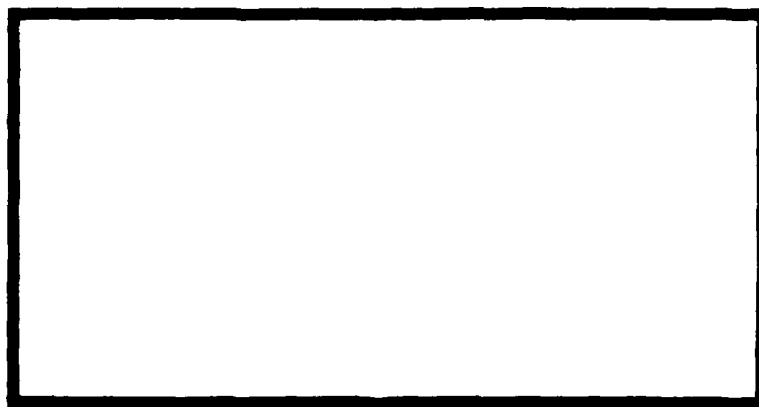
①



DTIC
ELICITE

FEB 18 1982

E



ENC. FILE COPY

UNITED STATES AIR FORCE
AIR UNIVERSITY
AIR FORCE INSTITUTE OF TECHNOLOGY
Wright-Patterson Air Force Base, Ohio

This document has been approved
for public release and sale; its
distribution is unlimited.

82 02 18 053

AFIT/GAE/AA/81D-27

LEVEL II

①

INVESTIGATION OF A TWO-DIMENSIONAL
MODEL FOR THE PREDICTION OF STATIC
DISPLACEMENT FOR T-38 HORIZONTAL
STABILATORS USING NASTRAN
THESIS

AFIT/GAE/AA/81D-27 JACK O. SAWDY
CAPT USAF

Approved for public release; distribution unlimited

INVESTIGATION OF A TWO-DIMENSIONAL MODEL FOR THE
PREDICTION OF STATIC DISPLACEMENT FOR T-38
HORIZONTAL STABILATORS USING NASTRAN

THESIS

Presented to the Faculty of the School of Engineering
of the Air Force Institute of Technology
Air University
in Partial Fulfillment of the
Requirements for the Degree of
Master of Science

by

Jack O. Sawdy, B.S.M.E.

Capt USAF

Graduate Aerospace Engineering

December 1981

Accession For	
NTIS	GRAB
DTIC	73
Unannounced	
Justification	
By	
Date	
Av	
Dist	
A	

Preface

My sincere thanks go to Capt H. C. Briggs for his guidance, patience, and extremely valuable suggestions given during the period of this study. The suggestions and guidance given by Dr. P. J. Torvik, Maj M. M. Wallace, and Capt A. R. Dewisplare were greatly appreciated.

I wish to thank the many personnel of the Air Force Wright Aeronautical Laboratory (AFWAL), in particular, Mr. S. Lustig, Mr. J. R. Pokorski, Mr. J. M. Curry, and ALC D. W. Resner, for their participation in the timely, successful completion of the data acquisition from the experimental test set-up documented by this thesis.

To my wife, Pat, my loving thanks for her understanding and support throughout the period of study, as well as, the many hours given for typing the pages herein.

Finally, appreciation goes to my special assistants, Laura and Jason, for leaving Dad to his studies.

Jack O. Sawdy

Contents

	<u>Page</u>
Preface	ii
List of Figures	v
List of Tables.	viii
List of Symbols	ix
Abstract.	x
 I. INTRODUCTION	 1
Purpose.	1
Background	2
Statement of the Problem	5
Approach to the Problem.	5
 II. SERIES 3 STATIC DEFLECTION TESTS	 6
Introduction	6
Test Apparatus	7
Data Acquisition Equipment.	12
Experimental Procedure	14
Data Reduction	15
Results.	16
 III. STABILATOR FINITE ELEMENT MODEL ANALYSIS	 17
Introduction	17
Development of the Finite Element Model.	18
Stabilator Description.	18
Substructure Elements	18
Boundary Conditions	23
Static Analysis.	23
Application of Optimization Theory.	26
Error Value Formulation	34
Variable Parameters Investigated.	36
 IV. RESULTS.	 39

Contents (Cont'd)

	<u>Page</u>
V. CONCLUSIONS AND RECOMMENDATIONS	42
Bibliography	44
APPENDIX A: Experimental Test Results	45
APPENDIX B: Graphic Presentation of Experimental Test Results	51
APPENDIX C: Data Generator FORTRAN Program Summary	62
APPENDIX D: Grid Point Identifications.	66
APPENDIX E: Alter Routine for Error Value Calculation	72
APPENDIX F: Two-Dimensional Model Versus Torsion Cell.	74
APPENDIX G: Graphic Presentation of NASTRAN Analytical Results.	78
Vita	89

List of Figures

<u>Figure</u>		<u>Page</u>
1	Series 3 Stabilator	3
2	Experimental Test Apparatus View 1.	9
3	Experimental Test Apparatus View 2.	10
4	Torque Tube Boundary Condition Measurement Apparatus	11
5	Hydraulic Pressure Source and Monitor Screen.	12
6	Data Acquisition Console.	13
7	Influence Coefficient Model Mesh.	19
8	Finite Element Model Coordinate Systems	22
9	Torsion Cell versus Two-Dimensional Model	38
B-1	Subcase 1 Experimental Deformation.	52
B-2	Subcase 2 Experimental Deformation.	53
B-3	Subcase 3 Experimental Deformation.	54
B-4	Subcase 4 Experimental Deformation.	55
B-5	Subcase 5 Experimental Deformation.	56
B-6	Subcase 6 Experimental Deformation.	57
B-7	Subcase 7 Experimental Deformation.	58
B-8	Subcase 8 Experimental Deformation.	59
B-9	Subcase 9 Experimental Deformation.	60
B-10	Subcase 10 Experimental Deformation	61
D-1	Grid Point Identification GP 1 to GP 27	67

List of Figures (Cont'd)

<u>Figure</u>		<u>Page</u>
D-2	Grid Point Identification GP 19 to GP 63	68
D-3	Grid Point Identification GP 55 to GP 99	69
D-4	Grid Point Identification GP 91 to GP 126.	70
D-5	Grid Point Identification GP 118 to GP 166	71
F-1	Diamond Shape Approximation of Airfoil	74
F-2	Thin Rectangular Shape Approximation for FEM.	74
G-1	Subcase 1 NASTRAN Analytical Deformation Due to a 382 lb Load at GP 147	79
G-2	Subcase 2 NASTRAN Analytical Deformation Due to a 382 lb Load at GP 151	80
G-3	Subcase 3 NASTRAN Analytical Deformation Due to a 682 lb Load at GP 152	81
G-4	Subcase 4 NASTRAN Analytical Deformation Due to a 382 lb Load at GP 153	82
G-5	Subcase 5 NASTRAN Analytical Deformation Due to a 782 lb Load at GP 156	83
G-6	Subcase 6 NASTRAN Analytical Deformation Due to a 1182 lb Load at GP 157.	84
G-7	Subcase 7 NASTRAN Analytical Deformation Due to a 782 lb Load at GP 158	85
G-8	Subcase 8 NASTRAN Analytical Deformation Due to a 1182 lb Load at GP 160.	86
G-9	Subcase 9 NASTRAN Analytical Deformation Due to a 1182 lb Load at GP 104.	87

List of Figures (Cont'd)

<u>Figure</u>		<u>Page</u>
G-10	Subcase 10 NASTRAN Analytical Deformation Due to a 1182 lb Load at GP 106	88

List of Tables

<u>Table</u>		<u>Page</u>
I	Series 3 Stabilator Parts List	4
II	Experimental Apparatus	8
III	Analytical Load Cases.	24
IV	Experimental Displacements	46

List of Symbols

BDATA	<u>Bulk Data</u> Deck FORTRAN Program
C	Chord length (inches)
CBAR	NASTRAN beam structural element
CQUAD1	NASTRAN 4-sided membrane structural element
CTRIA1	NASTRAN 3-sided membrane structural element
E	Young's Modulus
FS	Fuselage station
G	Shear modulus
GP	Grid Point (NASTRAN)
HSS	Horizontal stabilator station
I	Bending Moment of Inertia
J	Torsional Moment of Inertia
lb	Pound(s)
mv	Milli-volt(s)
NASTRAN	<u>NASA Structural Analysis</u>
No	Number(s)
rad	Radian(s)
SPC	Single Point Constraint
t	Thickness (inches)
v	Volt(s)
WL	Water line station

Abstract

This report documents the results of the experimental tests performed on a T-38 horizontal stabilator and the investigation of a two-dimensional finite element model for prediction of static displacement using NASA structural analysis (NASTRAN) computer program. The finite element model was used in previous and concurrent theses efforts with regard to T-38 flutter prediction via NASTRAN modal analysis methods. It will also be used in future analyses by a Using Air Force Agency for flutter prediction.

The experimental test set-up for the stabilator measured the displacements in the downward (water line) direction for ten load conditions with the displacements measured at twenty-five locations for each of the loading conditions. Precision load cells were used to measure the applied load and the resistance to rotation at the actuator arm. The boundary conditions of the tests represented an asymmetric loading condition for the T-38 assemblage.

The need for an improved two-dimensional finite element model was based on the results of previous flutter investigations using the same two-dimensional model. The model was to be used to analyze degradations in flutter speed due to repair. It was postulated that by optimizing the model characteristics for the static displacement cases that the improved model would better predict the flutter speed also.

The results of the experimental tests were compared with those developed using NASTRAN. Several of the model characteristics were altered and investigated as to their effect on the prediction of the static displacement. The analytical displacements were compared with those achieved experimentally.

Finally, development of an optimization procedure is presented, as well as its application to tuning the finite element model. The development of the optimization routine was based on current information for optimization techniques. A comparison is drawn between the error value used herein and current optimization theory.

INVESTIGATION OF A TWO-DIMENSIONAL MODEL
FOR THE PREDICTION OF STATIC DISPLACEMENT
FOR T-38 HORIZONTAL STABILATORS USING NASTRAN

I Introduction

Purpose

The horizontal stabilator of the United States Air Force T-38 Talon supersonic jet trainer (henceforth, referred to as stabilator) is the subject of this thesis. San Antonio Air Logistics Center (SAALC) currently has primary engineering responsibility for repair and maintenance of the T-38 stabilator. SAALC has the requirement for an improved method of examining the vibration modes and frequencies for flutter speed prediction of repaired stabilators. A two-dimensional finite element model (FEM) was developed to further analyze the modal frequencies of the stabilator using NASTRAN. The use of modern computer numerical analysis methods (NASTRAN) represented an improvement over traditional methods of analysis using strip theory. However, the accuracy of NASTRAN's capability to predict static displacements and modal frequencies (thus predicting the flutter speed) is directly related to the input information contained in the bulk data deck of the FEM. Therefore, it is the purpose of this thesis to investigate the two-dimensional finite element model characteristics for predicting static displacements for the T-38 horizontal stabilator using NASTRAN.

Background

Two stabilators were built by Northrop Aircraft, Inc. (Northrop) for T-38 usage, designated Series 2 and Series 3. Initial development and testing was performed on the Series 2 stabilator containing three auxiliary ribs which were deleted from the Series 3 design. However, the stabilator in use currently is the Series 3 design. Thus, a void in the data for proper deflection analysis based on the Series 3 configuration existed (for both static and dynamic conditions). The research and analysis presented herein was developed using the Series 3 stabilator only (Fig 1, Table I).

The two-dimensional FEM has been used by previous thesis students John O. Lassiter (Ref 1) and Roger K. Thomson (Ref 2) for use in flutter analysis. In each of the above studies, reference was made to the discrepancy in static displacements (from NASTRAN verification computations) when compared with published Northrop test results. Speculation was made as to the probable causes. Cited were possible FEM errors and the lack of applicable experimental data for comparison of static deflection verification. It was a logical extension of the previous theses efforts to perform the needed experimental tests for static deflections and attempt to refine the FEM for the static displacement case.

It is assumed the reader has an adequate background or working knowledge of NASTRAN or other finite element methods for structural analysis with particular emphasis in the solution techniques employed in static deformation problems.

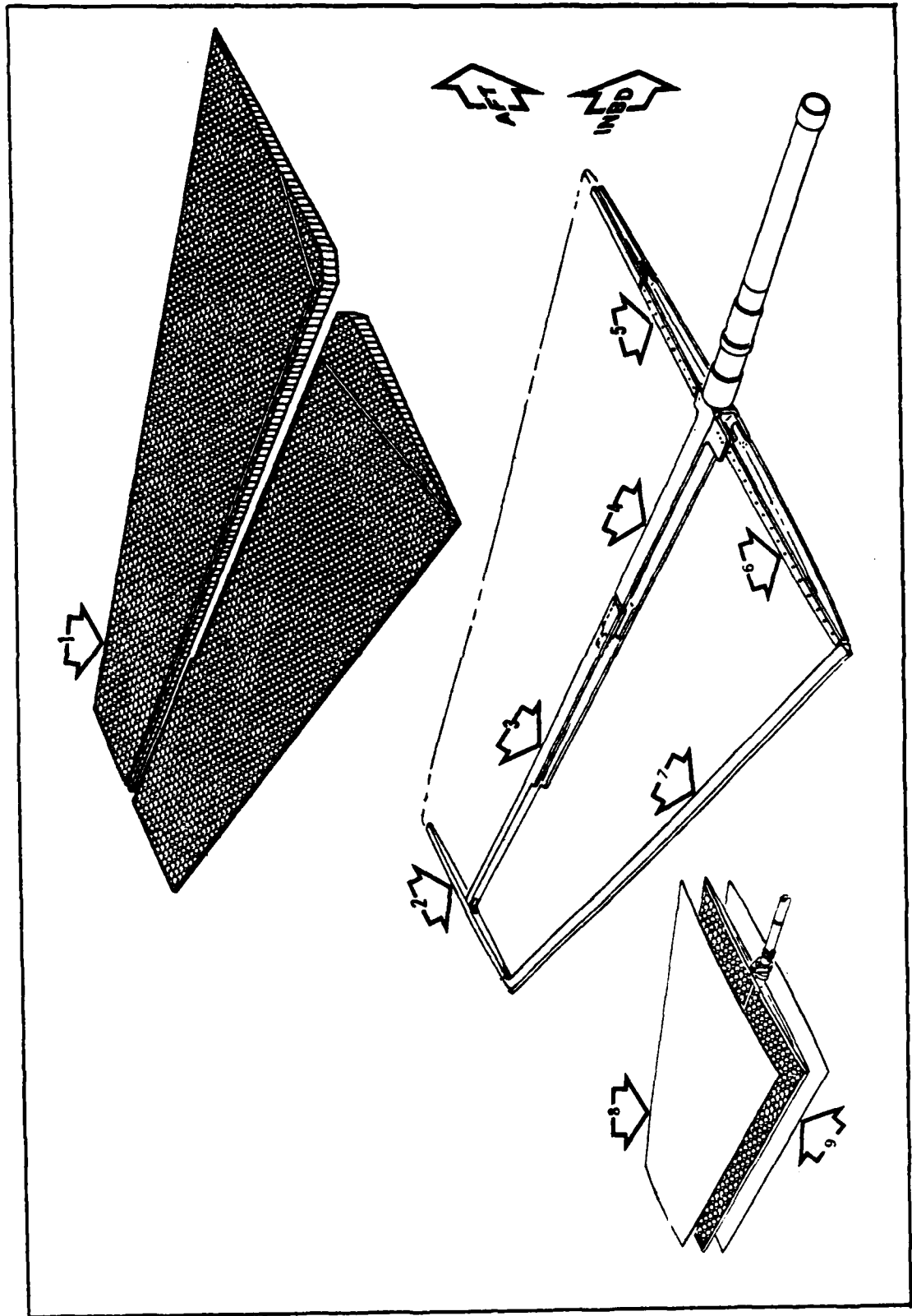


Figure 1. Series 3 Stabilator

TABLE I

Series 3 Stabilator Parts List (Ref 3: Sec IV)

Index No.	Part No.	Nomenclature	Gage	Material
1	3-32350	Honeycomb Core	0.0007 P Foil 0.125 Cell	Aluminum Alloy 5052-H39
2	3-32353	Rib	Machined Bar	Bar Aluminum 7075-T6
3	3-32356	Main Spar	Machined Bar	Rolled Bar Aluminum Alloy 7075-T6
4	3-32317	Hinge Fitting	Machined Forging	Steel 43M30
5	3-32352	Rib	0.025 in, Forged	Sheet Alclad 7075-T6
6	2-32310	Rib	0.025 in, Forged	Die Forged Aluminum Alloy 2014-T6
7	3-32357	Leading Edge	Machined Plate	Plate Aluminum Alloy 7075-T6
8	3-32355	Upper Skin		Sheet Alclad 7075-T6
9	3-32355	Lower Skin		Sheet Alclad 7075-T6

Further, it would be of benefit in evaluating the results if the reader were knowledgeable in the area of flutter analysis; inasmuch as, the end goal of the FEM is to predict flutter speed for the T-38 based on stabilator vibration.

Statement of the Problem

Investigate the geometric and physical characteristics of the two-dimensional FEM used with NASTRAN to predict static displacement for a T-38 Series 3 stabilator, with the goal of minimizing the difference between analytical and experimental results.

Approach to the Problem

As inferred earlier, the lack of experimental data for deflection measurement of the Series 3 stabilator had created a problem in verifying the quality of the two-dimensional finite element model. The initial step to resolving the problem was to perform the necessary experimental tests on the Series 3 stabilator. Once the tests were accomplished and the results reduced, the next step was to accomplish a comparison between the results produced analytically using the Series 3 FEM with NASTRAN and the results achieved experimentally. Lastly, effects of varying model characteristics (eg. Young's Modulus, element inertia, thickness, etc.) were to be investigated with the goal of developing an optimum FEM for the NASTRAN prediction of static displacement. The optimized FEM would then be used for flutter prediction.

II Series 3 Static Deflection Tests

Introduction

The experimental tests were performed on a Series 3 stabilator (Fig 1). The tests paralleled that developed by Northrop (Ref 4) for the Series 2 stabilator. Significant deviations from the Northrop report were the pad size (96 sq in (Ref 4) vs 49 sq in (used herein)), several of the load conditions (maximum experimental load was 1200 lbs), the use of a load cell in place of the control system actuator ram, and the boundary conditions (use of self-aligning bearing in two places in a rigid structure). Because of the differences, it was impossible to correlate the two tests although the load locations and displacement measurement locations were the same. The applied load was measured in twenty percent increments and data recorded for each increment. By recording the data at each twenty percent of load, it was possible to check the linearity of any particular displacement measured. Also, each load was cycled a minimum of two times to reduce any possible hysteresis of the system before recording data. However, only the maximum load condition deflections were averaged and used for analysis comparison. Therefore, any further reference to a load or displacement is based on the maximum load value and its corresponding displacements. Presented in this section is a description of the experimental test apparatuses, data acquisition equipment, procedures used in acquiring the data, and data reduction.

Test Apparatus

The experimental tests were performed using the resources of the Air Force Wright Aeronautical Laboratories (AFWAL), building 65, Wright-Patterson AFB, Ohio (Table II). The structure used in supporting the stabilator for the tests was made of steel and aluminum components (Fig 2). "C" channel beams with riveted spacers formed "I" beam sections. These were bolted, with separate corner pieces, to form the support structure. The stabilator was supported using self-aligning bearings in aluminum fixtures. These were located on the torque tube at HSS 25.07 and HSS 0.00, outboard bearing and aircraft centerline positions, respectively. The self-aligning bearings were the same as those used in the aircraft. This represented an asymmetric loading condition. The stabilator was mounted such that the stabilator planform was parallel to the floor. This allowed the displacements to be measured vertically.

A two inch diameter ram was used to provide the displacement loads. The Revere precision load cell, connected to the ram, was calibrated to 1000 pounds with a load capacity of 1500 pounds. The pad used for load transfer was approximately fifty square inches (7 in by 7 in). A rod end joining the load cell to the pad allowed the pad to rotate as necessary to meet the surface angle of the stabilator. Thus, deviation of the ram from the plumbed position was insignificant. Hydraulic pressurization of the ram provided stabilator displacement (downward). However, it was possible to begin and end with zero displacement calibrations, since the ram could be lifted

TABLE II

Experimental Apparatus

Apparatus	Manufacturer	Model	Comments
Precision Load Cell	Revere	C-42412	2mV/V, 1K, dual bridge
Hydraulic Ram	Snyder/Curry		2 inch bore
Precision Load Cell	Toroid	35-233-GBDF	3mV/V, 2.5K, dual bridge
Dial Indicator	Starrett		2 inch dial, .001 increments
Displacement Transducer	Research	4046	1, 2, and 3 inch capacities potentiometric
Hydraulic Source	AFWAL/FIB		Manual pump tension - compression
Data Screen	TEC	EKA8849	Connected to PDP-11
Data Terminal	TEC	1401	Connected to PDP-11
Digital Voltmeter	American Measurement and Control	515	Bridge balance and power supply
Signal Conditioning Modules	Research	4094/4095	Potentiometric balance and power
Data Acquisition System	Dayton Scientific	RTP-7400	Sequential send/receive
Digital Computer	Digital Equipment Corporation	PDP-11	32K, on-line data processing

from the surface of the stabilator using return hydraulic pressure.



Figure 2. Experimental Apparatus View 1

Measurement of the displacement was made using potentiometric displacement transducers. The range of displacement made it necessary to use three sizes of transducers (1, 2, and 3 in). Twenty-five transducers were attached to a sub-frame located beneath the stabilator (Fig 3). Each transducer position was found using a plumb line from the attachment point on the stabilator. The transducers were attached to the stabilator via .016 inch stainless steel transmission wire. The twenty-five positions corresponded to those in Reference 4

testing. A manual jack located beneath the outboard bearing support structure served to enforce the zero bearing displacement boundary condition. Force in the downward direction (to enforce zero vertical displacement) was applied to the centerline bearing by way of tightening adjustment bolts on the support structure.

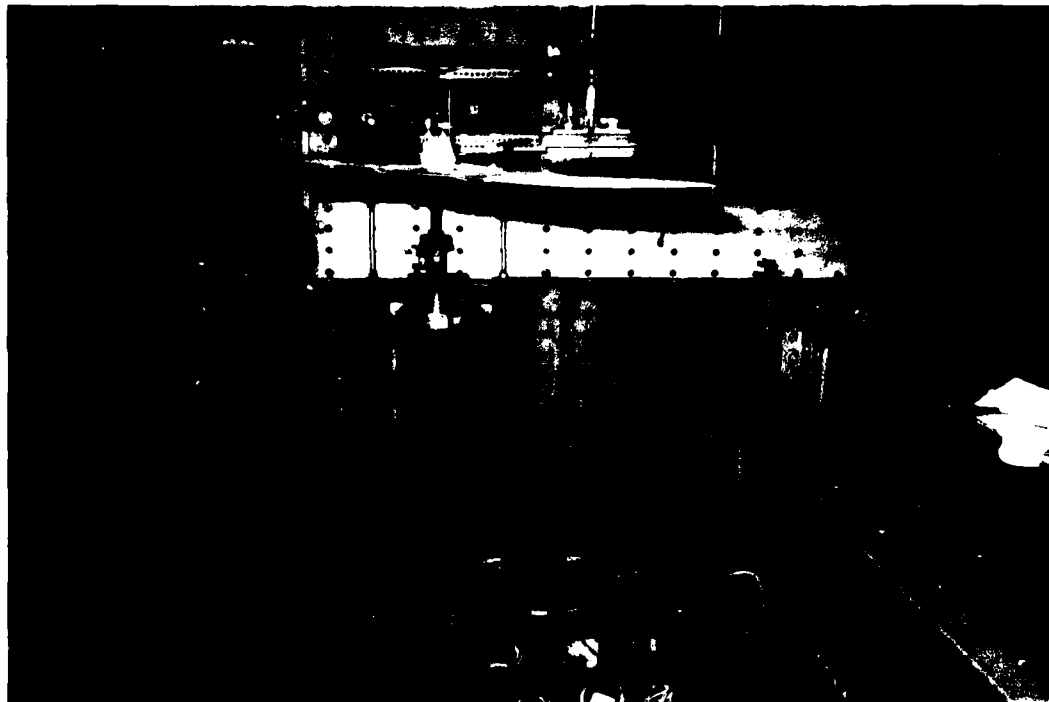


Figure 3. Experimental Test Apparatus View 2

Movement of the bearings (outboard and centerline) was monitored for vertical displacement via two inch dial indicator gages which read to one thousandth of an inch. The support brackets for the gages were attached to an assumed rigid structure (Fig 4). A Toroid precision load cell was

used to measure the reaction loads at the control actuator arm. The spring constant for the load cell was 5.0×10^5 pounds per inch. It was calibrated to 2500 pounds with a load capacity of 3750 pounds.



Figure 4. Torque Tube Boundary Condition Measurement Apparatus

Hydraulic pressure was obtained using manual pumps with internal reservoirs (Fig 5). The assembly was manufactured by AFWAL. Pressure gages monitored the line pressure as a safety precaution. Fine adjustment of the hydraulic pressure was obtained using a screw device to create small changes in hydraulic line pressure.

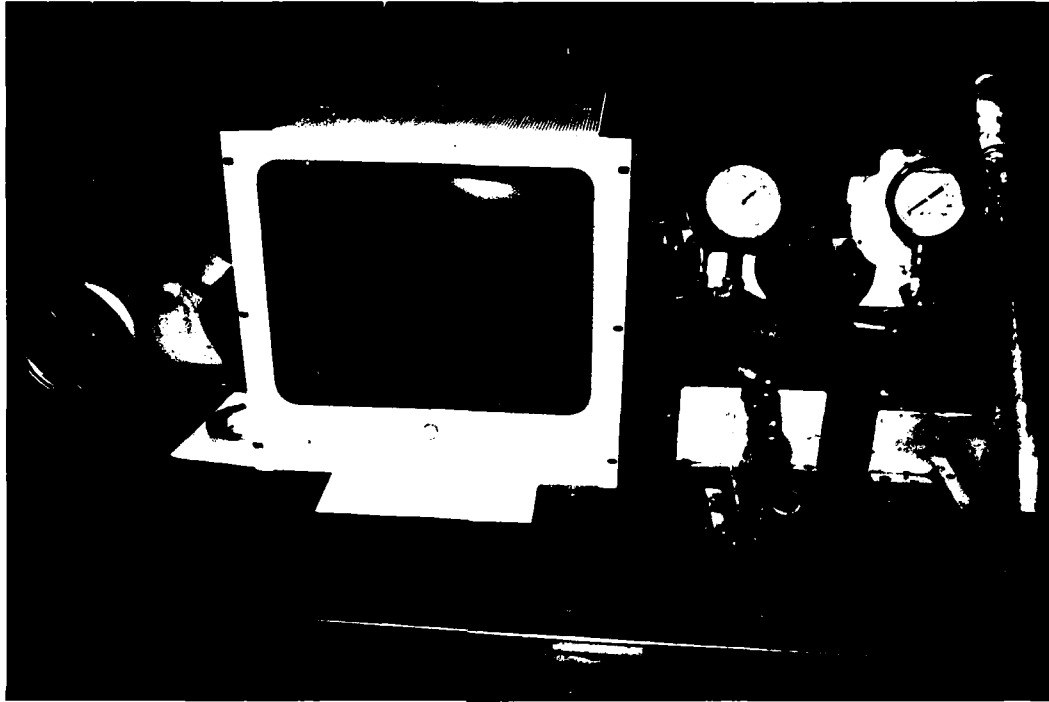


Figure 5. Hydraulic Pressure Source
and Monitor Screen

Data Acquisition Equipment.

A video screen was used to monitor the load on the stabilator at the hydraulic pump station. As a result of on-line data processing (in real time) it was possible to monitor the load (measured by the load cell), several displacements and adjust line pressure to the ram at the same station (Fig 5).

A separate grouping of apparatuses, shown in Figure 6, was assembled for data acquisition. The TEC terminal/screen was used to display the load cell values, displacements, and

interface with the PDP-11 computer for data processing. The PDP-11 digital computer was located in the same test building. A sample rate of five samples per second was selected for all tests, in as much as the tests were static displacement tests. Separate power and balance modules were used for each load cell and each transducer. An initial no load displacement reading of each transducer prior to load application was used as a zero reference. Zero displacement setting for each transducer was accomplished by displaying the voltages sent to the PDP-11 digital computer on the real time peripheral unit and adjusting the appropriate module for zero displacement (output voltage). A separate digital voltmeter was used for calibration readings for the load cells.

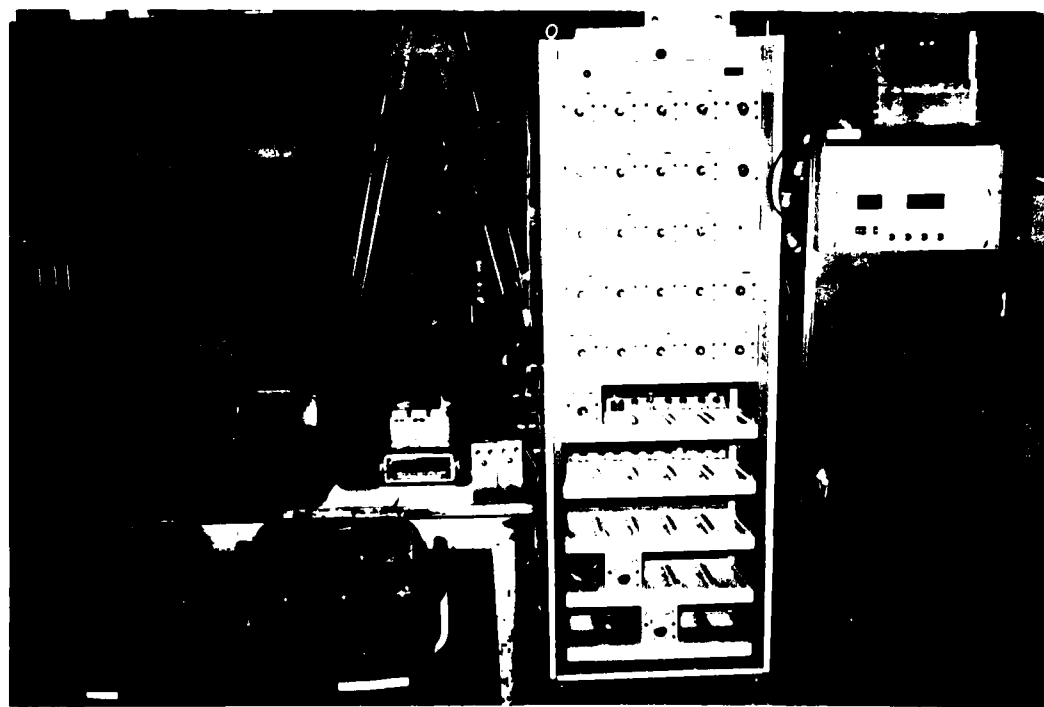


Figure 6. Data Acquisition Console

The Digital Equipment Corporation PDP-11 digital computer, housed in building 65, was used for data storage, sampling, and processing. The unit allowed for data to be read on the video monitors prior to its transfer to tape storage and post-processing. The data was processed on-line in engineering units in real time.

Experimental Procedure

The stabilator was placed in the support structure, previously discussed, using self-aligning bearings. The mid-thickness plane (planform) of the stabilator was parallel to the floor. The upper and lower surface load application and displacement locations were based on dimensions contained in Reference 3.

The position of each transducer was determined using a plumb line from the underside attachment fixtures. The displacement transducers were connected to the fixtures on the stabilator by fine stainless steel wire. The position of the torque tube height was checked and the dial indicators zeroed. The twenty-five transducers were then zeroed (relative position of the variable resistance transducer as measured by the real time peripheral unit was recorded by the PDP-11 as the start point for displacements with no load). The bridge balance on the load cells were checked and calibrated similarly.

The actuator position was determined by a plumb line from the overhead support beam to the position previously marked for a particular load application. Cross lines marking the position were used to center the pad. Gradual hydraulic

pressure was applied until contact of the rubber pad was made on the stabilator. Hydraulic pressure was increased and the applied load monitored on the video screens. The displacement of the torque tube was monitored and forced to zero vertically, using the mechanical jack and centerline bearing support adjustment fixture. The data was recorded for the applied load, reaction load at the actuator arm, and the twenty-five displacements for the particular load case. The load was then removed gradually, with the torque tube displacement continuously being held at zero vertically. The zero load residual displacements for the transducers were displayed (hysteresis effects). The process of calibrate, load, measure, unload was then repeated. When the system reached a hysteresis effect of less than five thousandths of an inch (for the worst case), the data was saved for post-processing, using commands from the TEC unit. One additional run was made for repeatability demonstration. This procedure was repeated for ten distinct load positions.

Data Reduction

Data recorded from the experimental tests were post-processed into tabular listings. The recorded data was saved at a rate of five samples per second. Since the tests were static, any variation in displacement was accounted for by averaging each transducer's output to establish a single value for displacement for a particular load condition.

A separate FORTRAN program was used to expand the experimental data by linear interpolation into a grid arrangement

which was the same as that used for NASTRAN computations. The interpolated displacement results were then used as input to the graphics computer code GCSNAST.

Results

The experimental tests were successful with respect to providing data for static deflections of the Series 3 stabilator. A correction to the input load measured at the ram was necessary, since the bridge balance for the load cell was accomplished with the pad suspended on the end. With this correction applied, good correlation was found between the applied load and the measured reaction load at the actuator arm.

Results of initial trial tests indicated a need for further support on the torque tube bearings to enforce zero vertical displacements. The use of a jack under the outboard bearing and a support structure with adjusting bolts above the centerline bearing solved the problem.

The measured displacements were averaged for each load condition. The results are presented in Appendix A. The displacements were then linearly interpolated to an expanded set of displacements. The linearly expanded set was then used with the computer graphics code GCSNAST to produce figures (App B). The figures illustrate the deformed shape and were useful in comparing the analytical results (which are discussed in the following chapter).

III Stabilator Finite Element Model Analysis

Introduction

The two-dimensional finite element model had been used in previous theses by Lassiter (Ref 1) and Thomson (Ref 2) as mentioned in Section I. A detailed description of the initial development of the FEM can be found in Reference 1, Section II and Appendix A. Those items significant to the development of this analysis will be presented here also. The data necessary to describe the physical characteristics of the stabilator for NASTRAN (part of the Bulk Data Deck) was generated from a separate FORTRAN program (BDATA). A description of the data generating program is presented in Appendix C. The elemental substructures used to model the stabilator were triangular membrane and bending elements (CTRIA1), quadrilateral membrane and bending elements (CQUAD1), and simple beam elements (CBAR) (Ref 5). In the interest of clarity and congruity, the FEM used herein was referred to as the influence coefficient model in the above theses. The number of elements, nodes, and physical dimensions for base line data were the same as those used in the influence coefficient model of previous theses.

The FEM boundary conditions were based on those modelling the experimental tests (not the same as the actual aircraft, previous Northrop tests, or other theses efforts).

Development of the Finite Element Model

Stabilator Description. The T-38 Talon stabilator is a lightweight, honeycomb structure with aluminum panels (upper and lower surface) bonded to the honeycomb core by epoxy. The aluminum panels are riveted to substructures, such as, the root rib, main spar, auxiliary spar, tip rib, and leading edge extrusion. When the stabilator is installed, the planform tilts four degrees down from the root rib to the tip rib.

Substructure Elements. NASTRAN, utilized in solving aerodynamic problems, had available the necessary elements to adequately model the stabilator. The plate bending elements with in-plane stiffness were used to model the skin-honeycomb core combination. These were the CQUAD1 and CTRIA1 elements. Bar elements (CBAR) were used to model the hinge fitting (torque tube and main spar), the auxiliary spar, tip rib, leading edge forging, root rib sections, and trailing edge closure (refer to Fig 1). It should be pointed out this combination of elements forms a two-dimensional FEM.

The influence coefficient model was developed based on 15 quadrilateral elements spanwise and 8 quadrilateral elements chordwise. Several quadrilateral elements were divided into triangular elements (Fig 7). The physical properties were found for the quadrilateral elements prior to being divided into triangular elements. The values of the physical properties at the four nodes were developed using the elemental properties at

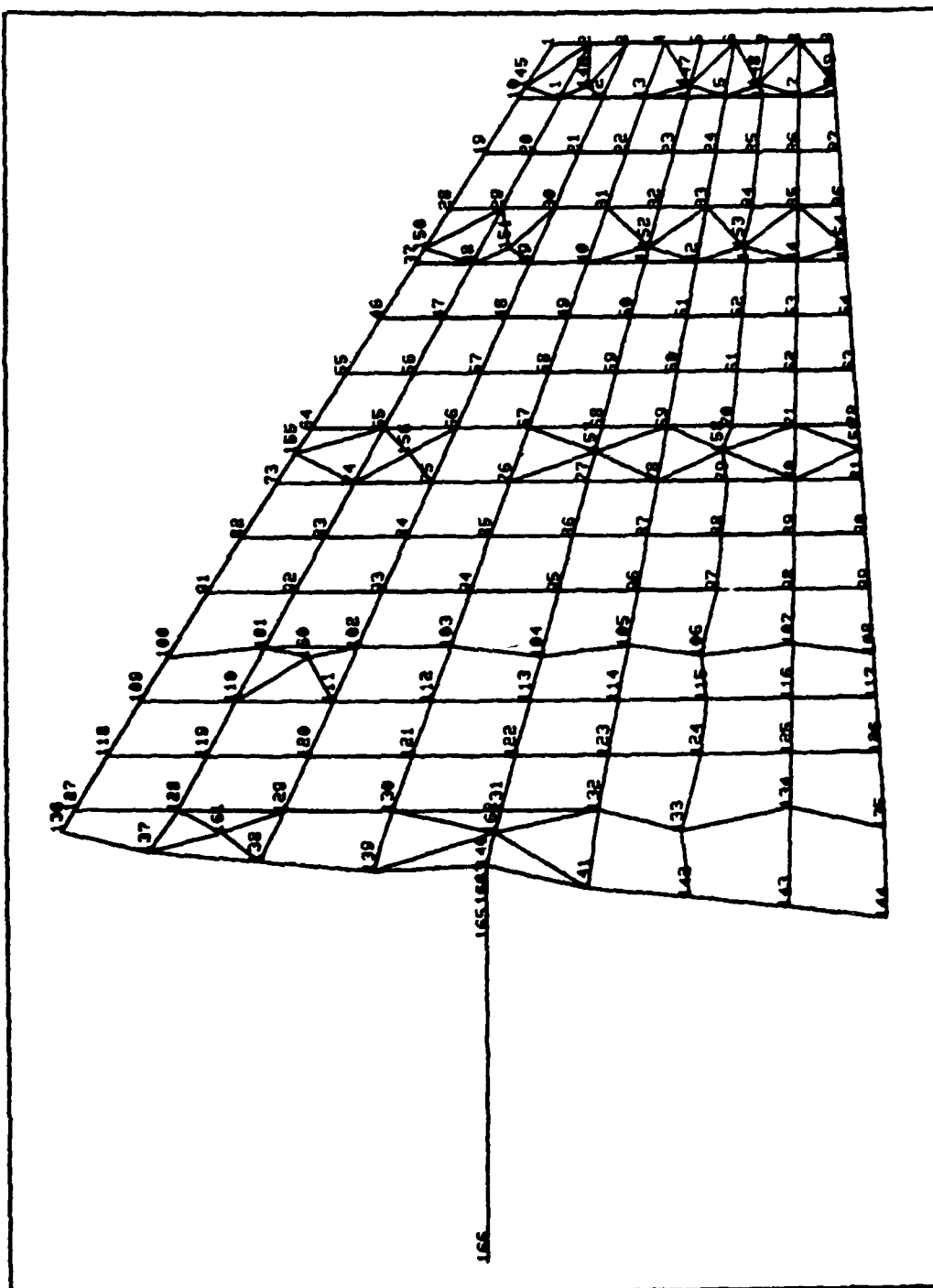


Figure 7. Influence Coefficient Model Mesh

the center of the element (found using a separate algorithm). The quadrilateral elements were then divided into triangular elements as required to form the influence coefficient mesh. Some nodes were moved to prevent poor aspect ratio triangles or for location of load application purposes. The resulting triangular elements or distorted quadrilateral elements used the same physical and material properties as were developed at the center of the quadrilateral element replaced.

Elemental properties for the bar elements were similarly formulated. The physical and material properties were determined at the center of the element and used for the entire element. The torque tube (a part of the hinge fitting - Fig 1) was developed separately. The location of the grid points were based on constraint requirements (eg. bearing locations, actuator arm location) and not on cross-sectional properties. The values used for physical properties were based on the dimensional characteristics of the section (three sections were utilized). Because of the complexity of the changing geometry of the torque tube between the root rib and the actuator arm location, averaged values were used for the sectional properties.

The program BDATA generated much of the data describing the physical and material properties used in describing the substructure elements. These included:

1. Property Cards (PBAR, PQUAD1, PTRIA1) identified the physical characteristics of the element, such as thickness, material identifiers, inertias, mass.

2. Material Cards (MAT1, MAT2) described the material characteristics, such as Young's modulus, shear modulus, Poisson's ratio. MAT1 was used for isotropic material. MAT2 was used for orthotropic material.

3. Grid points (GRID) were assigned unique geometric locations in terms of fuselage station (FS), horizontal stabilator station (HSS) and water line (WL) locations. GRID also identified the appropriate coordinate system and unique constraints for the grid point. The influence coefficient FEM used 166 grid points (App E).

4. Due to the four degree tilt of the planform in the aircraft installed configurations, a second coordinate system (CORD2R) was used for the planform (Fig 8). This permitted the loads to be applied normal to the planform and the displacements analyzed normal to the undeformed planform, duplicating the loading and measured displacement angles of the experimental tests.

Significant items of the FEM necessary for NASTRAN analysis which were not generated using BDATA are listed below.

1. The Executive Control Deck identified the solution format, as well as alterations for calculating an error value (App F).

2. The Case Control Deck contained information relative to controlling subcase solution sets and output requirements.

3. The single point constraints identifying constrained degrees of freedom at a grid point were used for fixed boundary conditions.

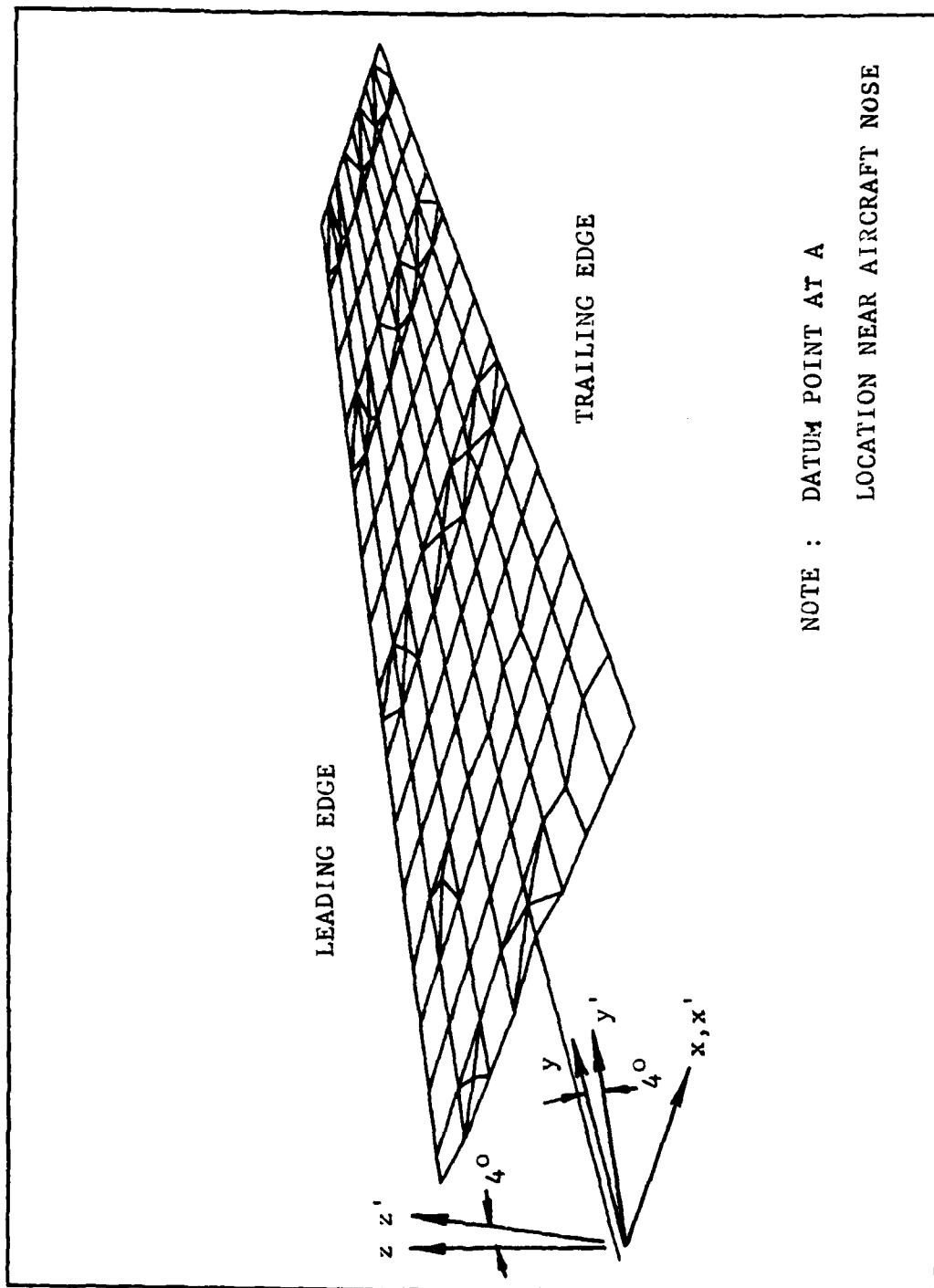


Figure 8. Finite Element Model Coordinate Systems

4. A scalar elastic element was used to model the load cell actuator arm.

5. The experimental values of the twenty-five node displacements were input for use in the Executive Control Deck Alter routine (App F).

6. Several other matrices were input for data extrapolation and matrix partitioning to be used by the Executive Control Alter routine (App F).

7. Lastly, the forces were input with directional cosines and appropriate coordinate system identification.

Boundary Conditions. The boundary conditions imposed on the FEM were based on the experimental tests. These represented an asymmetric loading condition as mentioned in the Introduction. A spring constant for the load cell-actuator arm was calculated from available data. The boundary conditions on the torque tube were rigidly fixed using single point constraints (SPC) for the x and z displacements at the outboard bearing and x, y and z displacements at the center-line bearing location.

Static Analysis

For static analysis of the FEM and the ten load subcases (Table III), Rigid Format 1 of NASTRAN was used. The mathematical formulation of the solution process is based on the linear theory of elasticity. The FEM stiffness matrix was formulated via the Bulk Data Deck (BDATA generated data and hand input data combined). The stiffness matrix was then

TABLE III

Analytical Load Cases

Case	Load	Grid Point No	Node No*	HSS	% Chord
1	382	147	3	82.00	52.7
2	382	151	7	70.75	20.0
3	682	152	8	70.75	52.7
4	382	153	9	70.75	75.0
5	782	156	12	56.50	20.0
6	1182	157	13	56.50	52.7
7	782	158	14	56.50	75.0
8	1182	160	17	42.25	20.0
9	1182	104	18	42.25	52.7
10	1182	106	19	42.25	75.0

* Ref 3 positions

partitioned with respect to constrained degrees of freedom and free degrees of freedom to be solved. Those equations not constrained, form a subset identified as the 1-set, which is the solution set for static analysis (Ref 6).

The influence coefficient model was developed as a result of the requirement that the load (force) be concentrated at a grid point for static analysis. The set of forces is reduced to a 1-set for nodal forces from constraint partitioning corresponding to the stiffness reduction. This reduces the solution process to that of satisfying equilibrium equations for stiffness versus force. The resulting equation can be expressed as

$$\{P\} = [S] \{\delta\}.$$

The vectors P and δ represent the nodal forces and displacements, respectively, and the matrix S represents the FEM stiffness matrix. For solution of the equations, NASTRAN reduced the stiffness matrix into its upper and lower triangular factors. Then forward-backward substitution is performed for all load cases having the same constraints, which was the case here. The displacement solution for each load case contained three translational and three rotational values for each grid point (except those displacements constrained). The vertical displacements for twenty-five grid points, to be compared with the experimental displacements, were extracted using an Alter routine in the Executive Control Deck section of the Bulk Data Deck (App F).

The results of the static analysis displacements and the experimental displacements were compared.

A comparison of the experimental reaction load and computed reaction load at the actuator arm was made. The reaction loads were found to be in excellent agreement after the magnitude of the applied load was corrected by subtracting the weight of the pad suspended from the load cell.

Application of Optimization Theory. As an introduction to the development and implementation of an error function for optimizing the difference between the computed displacements and the experimental displacements, several key optimization principles are reviewed (Ref 7). Several current computer programs used for implementation of optimization functions are also reviewed for possible future utilization.

Similar to most optimization formulations, the error in the displacements (or effectiveness of the system) was calculated from a number of individual subcases (sometimes only one case is optimized). Each of the subcases may also have effectiveness measurements associated with them. For the problem herein, the overall effectiveness might be expressed as

$$SE = \sum_{i=1}^n z_i(\underline{a}, \underline{x})$$

where z_i represents a performance indicator for the subcases

and is a function of \underline{a} and \underline{x} , the decision and state variables, respectively. This relationship is used to find the error (SE - system effectiveness). In this case, the minimum value is sought. Each of the subcases can be expressed functionally by relationships of the decision variables, such as

$$z_i = f_i(\underline{a}, \underline{x})$$

Thus,

$$z_1 = f_1(E, I, G, J, t, \text{ etc})$$

The functions developed for subcase performance identifiers relate the effects or sensitivity of the decision variables (\underline{a}) and state variables (\underline{x}) to the effectiveness measure for that particular subcase (z_i) - an extensive effort for ten subcases. The combination of decision variables and state variables must be capable of describing the state of the system (the error for the particular subcase z_i) for any variable (\underline{a} and/or \underline{x}) change, which in turn is used to establish the value of the system effectiveness.

For the analysis to be manageable, it is desirable that the performance index vector \underline{Z} (where $\underline{Z} = \{z_1, z_2, \dots, z_n\}$) have several basic properties. The vector \underline{Z} must be complete with respect to the system effectiveness. This reiterates the necessity for the decision variables and the state variables to describe the state of the system for any variable change. \underline{Z} should convey meaningful results (as it did herein - summing all the inches differences in displacements).

Z should be decomposable into generally independent elements. This relates to one of the problems found in the analysis; that is, changing one decision variable and having z_i values change with conflicting results (some improved - others became worse). To avoid having the SE biased, the relationships of the subcase identifiers (z_i) must be non-redundant. This avoids being rewarded (or penalized) twice or more for the same variable change. The size of the n-vector Z should be kept to a minimum. The recommendation here is to pick one dominant in spanwise bending, subcase (2); two dominant in chordwise bending, subcases (8 and 10, one for each rotation direction); one mixed mode, subcase (4); and one close to the boundary, subcase (9). This requires deleting five subcases (1, 3, 5, 6, and 7). This should make the optimization tractable, as well as feasible.

Once the necessary state variables are established, which accurately define the state of each subcase performance indicator, the value of the decision variables can be bounded for the decision space. The constraining equations (C_g) further limit the number of iterations necessary for a numerical solution. However, they should be of sufficient size to adequately consider all combinations for arriving at the optimum SE solution set. As an example, considering the development of an equivalent thin rectangular bar in rotation for replacing a torsion cell, Young's modulus might be made to vary from E to 4E. Expressing this as an inequality, the relationship would be

$$C_g(E) = E \leq C_E \leq 4E$$

There are no limits placed on the number of constraint equations (C_g) which can be utilized. For the problem herein, it is recommended the range be as constraining as is feasible, or extended in small increments as necessary.

In the event it is desirable to evaluate the problem on the basis of a preferred variable, then a resulting hierarchy (weighting) of the variables leads to a complete equivalent ordering of the performance indicators (z_i). Mathematically, this can be expressed as an alternative (individual realizations of the performance indicators) and is represented by

$$\underline{z}^1 \succ \underline{z}^2$$

to be read as alternative \underline{z}^1 is preferred to alternative \underline{z}^2 where \underline{z}^i represents the set of performance indices associated with the i th alternative. Further, this implies the functional relationship $f(z_i^1)$ is greater than or equal to $f(z_i^2)$ for all i , with $f(z_i^1)$ strictly greater than $f(z_i^2)$ for at least one i .

Definitive relationships between decision variables (often identified as state equations) further decrease the number of actual independent variables that can be used for optimization. These are represented as equalities (ST_h). One such example is

$$ST_h(E) = \frac{E}{2(1+\nu)} - G = 0$$

Only one variable (E or G) is necessary, the other is redundant (assuming isotropic material properties). The use of orthotropic material properties would allow the use of independent bending (two directions) and shear moduli, thus having three decision variables to use for optimization (assuming the two bending moduli are not coupled by Poisson's ratio).

The method of solution outlined from Reference 7 is optimization using multiple objective optimization theory (MOOT). Mathematically the MOOT process can be represented as:

$$\text{Extremize } SE = \text{extremize } f(\underline{Z}(x)) = f(\text{extremize } \underline{Z}(x))$$

$$\begin{aligned} \text{subject to: } C_g(\underline{a}, \underline{x}) &\leq 0 & g &= 1, 2, \dots, k \\ ST_h(\underline{a}, \underline{x}) &= 0 & h &= 1, 2, \dots, m \end{aligned}$$

Where extremize means to minimize the error value for the problem herein. The result of the optimization is a set of variables ($\underline{a}, \underline{x}$'s) which form a non-dominated solution (\underline{y}^*) set (NDSS) (provided a solution exists). A non-dominated solution (NDS) is defined as:

$$\underline{y}^* \text{ is a NDS iff } \nexists (\underline{a}, \underline{x}) \in X \supset$$

$$z_r(\underline{a}, \underline{x}) > z_r(\underline{y}^*) \text{ for some } r = 1, 2, \dots, n$$

$$z_s(\underline{a}, \underline{x}) \geq z_s(\underline{y}^*) \quad \forall s \neq r$$

Therefore, \underline{y}^* is a NDS containing optimum values for both

\underline{a} and \underline{x} , if and only if, there does not exist an $(\underline{a}, \underline{x})$ for the range space of decision and state variables (X); such that $z_r(\underline{a}, \underline{x})$ is better than $z_r(\underline{y}^*)$ for some $r = 1, 2, \dots, n$ decision variable; and $z_s(\underline{a}, \underline{x})$ better than or equal to $z_s(\underline{y}^*)$ for all s not equal to r . Allowing X to be the range space for all possible realizations of \underline{a} and \underline{x} (from possible combinations of r values), then \underline{y}^* is a specific realization from within the range space and is a candidate solution set.

The software for solving the equations to arrive at a solution for the NDSS exists in several formats depending on the type of optimization to be performed. Examples of such programs are PROCES (Ref 8) and AESOP (Ref 7) developed at the Air Force Institute of Technology. The standard format of the input for these programs are of the following form

$$\begin{aligned} \text{Extremize } \underline{Z}(\underline{a}, \underline{x}) &= [\underline{A}] \{ \underline{a} \} + [\underline{B}] \{ \underline{x} \} \\ \text{subject to } C_g(\underline{a}, \underline{x}) &\leq 0 \quad \text{for } g = 1, 2, \dots, k \\ \text{and } ST_h(\underline{a}, \underline{x}) &= 0 \quad \text{for } h = 1, 2, \dots, m \end{aligned}$$

where $\underline{Z}(\underline{a}, \underline{x})$ is the performance vector, \underline{a} and \underline{x} are the decision and state variables, respectively, and A and B are matrices of coefficients relating the decision and state variables to the performance indices. The solutions satisfying the above relations are then compared with one another through a separate algorithm which checks for dominance. If the second candidate set $(\underline{a}, \underline{x})^2$ is better than the first candidate set $(\underline{a}, \underline{x})^1$, the second is retained

as a new NDS (y^*). This process continues until all candidate solution sets have been compared. The result is a NDSS, or the best solution set based on the relationships input, constraint equations, and state equations. Implementation of the vector optimization process is accomplished by the mathematical formulation

Extremize SE = extremize $f(\underline{Z}(\underline{a}, \underline{x})) = f(\text{extremize } \underline{Z}(\underline{a}, \underline{x}))$
reposed as

$$\begin{array}{ll} \text{Extremize } z_l(\underline{a}, \underline{x}) & \text{subject to:} \\ C_g(\underline{a}, \underline{x}) \leq 0 & \text{for all } g \\ ST_h(\underline{a}, \underline{x}) = 0 & \text{for all } h \end{array}$$

Formulating the solution using the constraint method, requires all other performance indices to be expressed as state equations, such as

$$z_k(\underline{a}, \underline{x}) - r_k = 0 \quad \text{for all } k \neq l \text{ above}$$

The constraint solution process optimizes one functional relationship while all other relationships are held constant. Where the range of all possible realizations for r_k depend upon the range of the individual objective functions. Optimization is accomplished sequentially for all possible values of r_k (and combinations thereof). The candidate solutions are compared as before to determine if a NDS exists (or no solution set is found due to the problem

being over constrained). Then, the system effectiveness is calculated based on the summation of the $z_i(\underline{a}, \underline{x})$ functionals from the optimum solution set of variables $(\underline{a}, \underline{x})$. If the constraint method proves to be ineffective for the problem at hand, the weighting method may be a feasible alternative. However, the weighting method may arrive at a solution set at the cost of some numerical accuracy.

Several factors deemed the above programs unusable for application (at the time analysis) to the problem presented herein. These included:

1. Assuming non-linear relationships of the decision variables could be derived, it would have required an excessive number of relationships to develop the minimization optimizing functions for the problem herein. None of the relationships could be deduced based on physical properties. The relationships developed would have to relate a change of decision or state variable with a displacement difference (versus pure displacements found in a static analysis problem).
2. The constraining equations necessary to search the entire domain of possible realizations were unknown. Thus, the range would be extensive for searching for the optimum solution set.
3. The state variable relationships were also unknown and could not be determined from physical insight of the problem.
4. AESOP (ability to handle non-linear relationships) was being developed concurrent with this thesis effort.

However, much of the optimization material presented was applied in deriving a method of error analysis for the stabilator. The major differences are noted as development of the error value formulation is presented.

Error Value Formulation. An error value function based on optimization principles was applied to the problem herein. The error value was formulated mathematically based on the minimization of the system effectiveness value. In theory, the minimum value of each of the subcases (z_j) resulted in the overall error value (E) being minimized.

$$E = \text{minimum} \sum_{j=1}^{10} z_j = \sum_{j=1}^{10} \text{minimum } z_j$$

Where E is the error (equivalent to SE in this application) in the FEM (analytical versus experimental). In reality, it was found that comparing the difference in displacement for the system effectiveness resulted in the error value being overly sensitive to the planform orientation and relatively insensitive to the planform curvature. Each subcase was equally weighted in the summation of the separate subcases. The subcase error value was a function of the difference between the analytical displacement and the experimental displacement. Mathematically, this was expressed as

$$z_j = \left[\sum_{i=1}^{25} (d(\underline{a}, \underline{x})_{ij} \text{ NAS} - d_{ij} \text{ EXP})^2 \right]^{1/2}$$

Where $d(\underline{a}, \underline{x})_{ij \text{ NAS}}$ represented the analytical (NASTRAN) displacements which were functions of the decision variables (\underline{a}) and the state variables (\underline{x}), and $d_{ij \text{ EXP}}$ represented the experimental displacements. The analytical displacements were replaced by the inverted stiffness matrix and forces

$$d(\underline{a}, \underline{x})_{ij \text{ NAS}} = \sum_{k=1}^{25} S(\underline{a}, \underline{x})_{ik}^{-1} P_{kj \text{ NAS}}$$

Where the stiffness matrix (S) would contain the decision variables (\underline{a}) and state variables (\underline{x}). The load cell spring constant was included as a decision variable in the stiffness matrix. The subcase performance indices can be reposed mathematically as

$$z_j = \left[\sum_{i=1}^{25} \left[\left(\sum_{k=1}^{25} S(\underline{a}, \underline{x})_{ik}^{-1} P_{kj \text{ NAS}} \right) - d_{ij \text{ EXP}} \right]^2 \right]^{\frac{1}{2}}$$

The subcase error value can then be evaluated for a solution set by varying the decision variables, subject to any constraining equations and state variable relationships.

However, no state variable relationships were identified for the problem herein and no constraints were imposed in the initial searches for candidate solutions. Thus, the resulting error function was

$$E = \sum_{j=1}^{10} \left[\left[\sum_{i=1}^{25} \left[\left(\sum_{k=1}^{25} S(\underline{a}, \underline{x})_{ik}^{-1} P_{kj \text{ NAS}} \right) - d_{ij \text{ EXP}} \right]^2 \right]^{\frac{1}{2}} \right]$$

A candidate solution set was used in the reduced error value function in determining the system effectiveness for the decision variables. The error calculated represented the sum of the difference in calculated vertical displacements versus experimental displacements for 250 data points (10 subcases, 25 data points per subcase). The Alter routine used in the NASTRAN analysis for compiling the comparison data (error value) is presented in Appendix E. The error for an individual subcase was useful in distinguishing relative error between spanwise bending and chordwise bending (psuedo-torsion). The boundary parameters were a significant factor in reducing the error value.

Variable Parameters Investigated. The problem of tuning the FEM to predict the experimental results was segregated into two distinct problem areas. The first was to resolve the dissimilarities in boundary parameters of the experimental results and the analytical results. The spring constant calculated for the actuator arm rotation was calculated to be 15.55×10^6 in lb/rad. This was the result of the actuator arm length of 6.0 inch with an equivalent spring constant of 3.2×10^6 lb/in at the actuator attachment end (Ref 9) combined with a reaction load cell spring constant of 5.0×10^5 lb/in. However, the spring constant which yielded the smallest error value (all other variables held constant) was 1.15×10^6 in lb/rad. The decision to use the boundary parameter values which optimized the analytical model was based on the goal of optimizing the planform deformation for flutter prediction usage

and the experimental boundary conditions were not those of the aircraft configuration. Once an optimum set of boundary parameter values were found, then the deformation of the stabilator planform was compared to the experimental displacements for optimization.

The variables used to establish the boundary conditions for rigid planform tilt and rotation were bending inertia of the torque tube sections (part of the hinge fitting) and the spring constant, respectively. They were iteratively adjusted as the planform variables were altered. Three basic parameters were investigated with respect to optimizing the FEM planform for analytical displacement prediction. They were inertias of the membrane elements in the spanwise and chordwise directions and the ratio of thickness to chord length. Bending in the chordwise direction was associated with a psuedo-torsion of the airfoil to distinguish it from bending spanwise.

Previous investigations were accomplished using isotropic elements. Appendix F develops the theory illustrating the need for orthotropic material properties to model the torsional shear flow when the FEM becomes a two-dimensional (planform) model (Fig 9). Computations were made using isotropic and orthotropic material properties.

The thickness to chord ratio variable was used as an effective weighting factor for proportioning both bending and psuedo-torsion effects. Since the thickness was divided by the chord length, any increase to the thickness



with Torsion Cell



without Torsion Cells

Figure 9. Torsion Cell Versus
Two-Dimensional Model

was equivalent to changing the airfoil shape. As an example, an increase in this variable resulted in proportional increases in bending inertias (both directions) at the thickest (Y direction) point on the chord, tapering to a minimum (zero) at the edges for a particular chord. Since the airfoil also tapers from the root rib to the tip rib, the effective weighting in thickness was also realized spanwise.

IV Results

Although the stabilator was restrained in a relatively rigid steel and aluminum structure, some displacement error was evident from the hysteresis recorded during the experimental tests. The data hysteresis was zero in most cases and repeatability was excellent. The maximum deviation for any particular load, displacement combination was found to be .004 inch. The data was averaged to arrive at the final results presented in Appendix A. The tabular results were then used as base line static displacement data for the Series 3 stabilator and all subsequent results herein. Static analysis of the reaction load at the load cell was found to be in excellent agreement with the applied load.

Many computations were made using the scalar error value as a measure of the accuracy of the FEM for static displacement. Since the error value represented the total difference (in inches) between NASTRAN predicted displacements and experimental displacements of the planform, it was found that variations in the boundary elements (torque tube and load cell) overwhelmed the effects of varying the physical parameters of the planform. There was a problem of having too many subcases to match displacements, and not enough physical relationships to equate some of the subcases (reducing the independent comparisons), thus, implying the scalar error function was too sensitive to planform orientation and insensitive to the problem of optimizing the planform deformation.

The goal was to determine the variables and their magnitudes for optimizing the two-dimensional FEM for eventual modal vibration analysis. The boundary element variables were reevaluated after each iteration of the planform variables to determine if further improvement in the scalar error value could be made. The boundary parameter values producing the best scalar error value were significantly different than those modelling available, reliable data.

As stated earlier, the rotational spring located on the torque tube to restrain the rotation was computed as 15.55×10^6 in lb/rad but the lowest scalar error value was found when a value of 1.18×10^6 in lb/rad was used. A comparison of the displacements at grid point (GP 151) was used to optimize the bending inertia necessary in the torque tube. It was found that the torque tube needed to be more flexible in bending by a factor of approximately 0.8 for the best planform orientation. This value was based on all other variables being held constant, and the optimum spring constant.

With the above changes in boundary variables, the planform of the stabilator was investigated. Variables used to optimize the planform curvature were orthotropic bending moduli material properties for spanwise and chordwise changes and the thickness to chord ratio. Curvature of the planform chordwise and spanwise could be altered independently using the plate bending moduli. Thickness to chord ratio changes were used when comparison of the data indicated the center

(approximately along the spar) should be stiffer (more heavily weighted) than the edges. FEM displacement errors at the four corners of the planform and several middle grid points were used to determine the bending and psuedo-torsion changes needed. Effects of thickness to chord ratio changes were investigated and found to adversely affect the results obtained using orthotropic properties.

The overall results indicated it was necessary to change the spanwise bending modulus by increasing its value by two percent. The chordwise bending modulus (psuedo-torsion) was increased by 200 percent (or 3 times the original value). The ratio of the thickness to chord length ratio was not changed. When combined with the optimum torque tube bending inertia and actuator arm spring constant, the scalar error was found to be 1.6 (i.e. 1.6 inches of displacement error in 250 data points). Prior to any optimization attempts, a scalar error of 10.4 was found. Optimization of the boundary elements accounted for lowering the scalar error to 1.8, prior to investigating the planform variables. Graphic presentation of the NASTRAN analytical results is presented in Appendix G.

V Conclusions and Recommendations

The thesis investigated a two-dimensional FEM for the prediction of static displacement for a T-38 horizontal stabilator using NASTRAN. Experimental data was obtained for a Series 3 stabilator. The data provided an adequate base of information for comparison purposes. A method of comparison was developed following current optimization principles. The scalar error value gave a measure of the effectiveness of the changes imposed on the combination of boundary parameters and planform parameters. It was found that the error function was too sensitive to planform orientation, since a lower scalar error value was not an indication that all subcases were being optimized. This feature was used to determine the optimum boundary element values by finding the boundary element values which minimized all subcases.

Orthotropic material properties were essential to the ability of tuning the model bending properties in the spanwise and chordwise directions independently. This was not used in previous theses efforts. The optimization process considered relatively few variables for use in tuning the model, considering the large number of elements and combinations which were used developing the FEM. However, many computations were required to narrow the results to an apparent optimum solution set. Based on the original model analyzed and the tuning technique used (scalar error value

optimization), the FEM using orthotropic plate elements (appropriately proportioned) represents a good stabilator finite element model.

One data point not acquired during the experimental tests was planform rotation. This would have been of great benefit in determining the optimum boundary parameter value for establishing planform rotation. It is recommended any further tests, which parallel the tests herein, include a method for recording the planform rotation.

It is recommended the results of this thesis be considered for vibration analysis of the T-38 stabilator. It is recommended that further investigation of the torque tube (part of the hinge fitting) be performed for its contribution to stabilator flutter. This recommendation is based on the large relative changes in the scalar error value attributed to varying the torque tube bending inertia and the attached load cell spring constant.

Bibliography

1. Lassiter, John O. Initial Development for a Flutter Analysis of Damaged T-38 Horizontal Stabilators Using NASTRAN. Wright-Patterson AFB, Ohio: Air Force Institute of Technology, March 1980.
2. Thomson, Roger K. Investigation of an Improved Flutter Speed Prediction Technique for Damaged T-38 Horizontal Stabilators Using NASTRAN. Wright-Patterson AFB, Ohio: Air Force Institute of Technology, December 1980.
3. T.O. 1T-38A-3. "Horizontal Stabilator Damage Repair," T-38 Maintenance and Repair Manual. Kelly AFB, Texas: San Antonio Air Logistic Center.
4. NOR-60-6. Static Test of Complete Airframe for the T-38A Airplane. Hawthorne, California: Northrop Aircraft, Inc., March 1960.
5. NASA SP-222(05). The NASTRAN User's Manual, Level 17.5. Washington DC: Scientific and Technical Information Division, National Aeronautics and Space Administration, December 1980.
6. Schaeffer, Harry G. MSC/NASTRAN Primer Static and Normal Modes Analysis. Milford, New Hampshire: Wallace Press, Inc., 1979.
7. Robinson, D.G. Notes from thesis development on optimization. Wright-Patterson AFB, Ohio: Air Force Institute of Technology, December 1981.
8. Dewisplare, A.R. "Algorithm Efficiency in Generating Non-Dominated Solution Sets," Proceedings of the IEEE 12th Annual Symposium on System Theory. Virginia Beach, Virginia: 1980. pages 281-222.
9. NAI 57-59. T-38A Horizontal Stabilizer Structural Analysis. Hawthorne, California: Northrop Aircraft, Inc., October 1958.
10. Aperture Cards (Code Identification Number 76823). Blueprints for the T-38 Horizontal Stabilator. Kelly AFB, Texas: San Antonio Air Logistics Center.
11. Timoshenko, S.P. and Goodier, J.N. Theory of Elasticity. New York: McGraw-Hill Book Co., 1970.
12. Budynas, R.G. Advanced Strength and Applied Stress Analysis. New York: McGraw-Hill Book Co., 1977.

Appendix A

Experimental Test Results

The following tables present the vertical deflections of the stabilator due to static loading. The location identification is given in terms of the NASTRAN grid point. Reference is also made to Northrop static displacement test locations in parentheses, which were used to establish load and deflection points.

The maximum applied load is presented. The applied load was the maximum recorded load minus the weight of the pad (8 x 8 x 1 inch steel plus rubber and attaching hardware, approximately 18 pounds). The reaction load was that measured by the load cell at the actuator arm for the maximum applied load.

The deflection data represents the average of the vertical displacements found for successive maximum loads. Positive is upward displacement, negative is down.

TABLE IV

Experimental Displacements

Position: Grid Point 147 (Ref 3, Node 3)						Applied Load: -382 lbs
Measured Actuator Arm Reaction Load: +939 lbs						
Percent Chord	82.0 HSS	70.75 HSS	56.50 HSS	42.25 HSS	30.0 HSS	
0.0	-0.983	-0.506	-0.159	+0.026	+0.185	
20.0	-1.086	-0.614	-0.236	-0.009	+0.087	
52.7	-1.153	-0.757	-0.382	-0.133	-0.020	
75.0	-1.325	-0.887	-0.461	-0.209	-0.097	
100.0	-1.453	-0.908	-0.534	-0.274	-0.168	

Position: Grid Point 151 (Ref 3, Node 7)					Applied Load: -382 lbs	
Measured Actuator Arm Reaction Load: +103 lbs						
Percent Chord	82.0 HSS	70.75 HSS	56.50 HSS	42.25 HSS	30.0 HSS	
0.0	-0.620	-0.419	-0.207	-0.055	+0.004	
20.0	-0.626	-0.436	-0.214	-0.058	-0.003	
52.7	-0.572	-0.395	-0.239	-0.079	-0.011	
75.0	-0.608	-0.430	-0.231	-0.078	-0.010	
100.0	-0.614	-0.399	-0.215	-0.062	-0.005	

TABLE IV (cont)

Position: Grid Point 152 (Ref 3, Node 8)						Applied Load: -682 lbs	
Measured Actuator Arm Reaction Load: +1332 lbs							
Percent Chord	82.0 HSS	70.75 HSS	56.50 HSS	42.25 HSS	30.0 HSS		
0.0	-1.150	-0.656	-0.225	+0.042	+0.265		
20.0	-1.247	-0.756	-0.325	-0.033	+0.134		
52.7	-1.289	-0.960	-0.527	-0.199	-0.035		
75.0	-1.471	-1.106	-0.639	-0.307	-0.141		
100.0	-1.611	-1.155	-0.760	-0.410	-0.254		

Position: Grid Point 153 (Ref 3, Node 9)						Applied Load: -382 lbs	
Measured Actuator Arm Reaction Load: +1180 lbs							
Percent Chord	82.0 HSS	70.75 HSS	56.50 HSS	42.25 HSS	30.0 HSS		
0.0	-0.621	-0.320	-0.063	+0.080	+0.237		
20.0	-0.727	-0.415	-0.152	+0.003	+0.124		
52.7	-0.807	-0.594	-0.323	-0.118	-0.017		
75.0	-0.960	-0.753	-0.438	-0.222	-0.116		
100.0	-1.105	-0.861	-0.573	-0.325	-0.227		

TABLE IV (cont)

Position: Grid Point 156 (Ref 3, Node 12)						Applied Load: -782 lbs
Measured Actuator Arm Reaction Load: -689 lbs						
Percent Chord	82.0 HSS	70.75 HSS	56.50 HSS	42.25 HSS	30.0 HSS	
0.0	-0.593	-0.500	-0.392	-0.237	-0.183	
20.0	-0.570	-0.441	-0.330	-0.181	-0.109	
52.7	-0.459	-0.370	-0.237	-0.091	-0.013	
75.0	-0.445	-0.324	-0.157	-0.016	+0.048	
100.0	-0.407	-0.226	-0.070	+0.061	+0.152	

Position: Grid Point 157 (Ref 3, Node 13)					Applied Load: -1182 lbs	
Measured Actuator Arm Reaction Load: +1552 lbs						
Percent Chord	82.0 HSS	70.75 HSS	56.50 HSS	42.25 HSS	30.0 HSS	
0.0	-0.977	-0.657	-0.251	+0.041	+0.298	
20.0	-1.073	-0.712	-0.350	-0.041	+0.147	
52.7	-1.069	-0.891	-0.566	-0.233	-0.040	
75.0	-1.239	-1.010	-0.692	-0.362	-0.168	
100.0	-1.353	-1.041	-0.820	-0.475	-0.312	

TABLE IV (cont)

Position: Grid Point 158 (Ref 3, Node 14)					
Measured Actuator Arm Reaction Load: +2192 lbs					
Percent Chord	82.0 HSS	70.75 HSS	56.50 HSS	42.25 HSS	30.0 HSS
0.0	-0.629	-0.365	-0.028	+0.178	+0.423
20.0	-0.759	-0.451	-0.164	+0.045	+0.226
52.7	-0.858	-0.700	-0.449	-0.183	-0.030
75.0	-1.035	-0.889	-0.677	-0.379	-0.210
100.0	-1.196	-1.001	-0.938	-0.609	-0.432

Position: Grid Point 160 (Ref 3, Node 17)					
Measured Actuator Arm Reaction Load: -2440 lbs					
Percent Chord	82.0 HSS	70.75 HSS	56.50 HSS	42.25 HSS	30.0 HSS
0.0	-0.280	-0.348	-0.441	-0.477	-0.548
20.0	-0.211	-0.232	-0.275	-0.304	-0.326
52.7	-0.067	-0.055	-0.039	-0.008	0.000
75.0	+0.056*	+0.069*	+0.123	+0.170	+0.193
100.0	+0.134*	+0.194	+0.307	+0.380	+0.443

*Max value (not at 100% applied load)

TABLE IV (cont)

Position: Grid Point 104 (Ref 3, Node 18)					
Measured Actuator Arm Reaction Load: +793 lbs					
Percent Chord	82.0 HSS	70.75 HSS	56.50 HSS	42.25 HSS	30.0 HSS
0.0	-0.353	-0.235	-0.087	+0.039	+0.163
20.0	-0.404	-0.279	-0.139	-0.006	+0.077
52.7	-0.417	-0.343	-0.241	-0.109	-0.016
75.0	-0.483	-0.405	-0.291	-0.176	-0.094
100.0	-0.535	-0.433	-0.362	-0.256	-0.181

Position: Grid Point 106 (Ref 3, Node 19)					
Measured Actuator Arm Reaction Load: +2979 lbs					
Percent Chord	82.0 HSS	70.75 HSS	56.50 HSS	42.25 HSS	30.0 HSS
0.0	-0.382	-0.151	+0.106	+0.312	+0.553
20.0	-0.499	-0.286	-0.056	+0.146	+0.310
52.7	-0.624	-0.519	-0.373	-0.176	-0.030
75.0	-0.782	-0.713	-0.599	-0.475	-0.299
100.0	-0.936	-0.837	-0.871	-0.833	-0.664

Appendix B

Graphic Presentation of Experimental Test Results

A separate FORTRAN program was used to generate a displacement deck which could be read by GCSNAST (a NASTRAN graphics support code). The program expanded the experimental displacement mesh size from twenty-five nodes to 166 grid points using linear interpolation between the nodes. The output results of the program were then used as input to GCSNAST for graphic presentation of the experimental results presented in this appendix.

The views illustrated present the same view as the experimental tests set-up (shown in Figs 2 and 3). The two-dimensional FEM forms a reference plane (horizontal line) for the undeformed stabilator, such that the leading edge is to the left and the trailing edge is to the right. Reference loading is maximum recorded load (not applied load value). Load position is also noted.

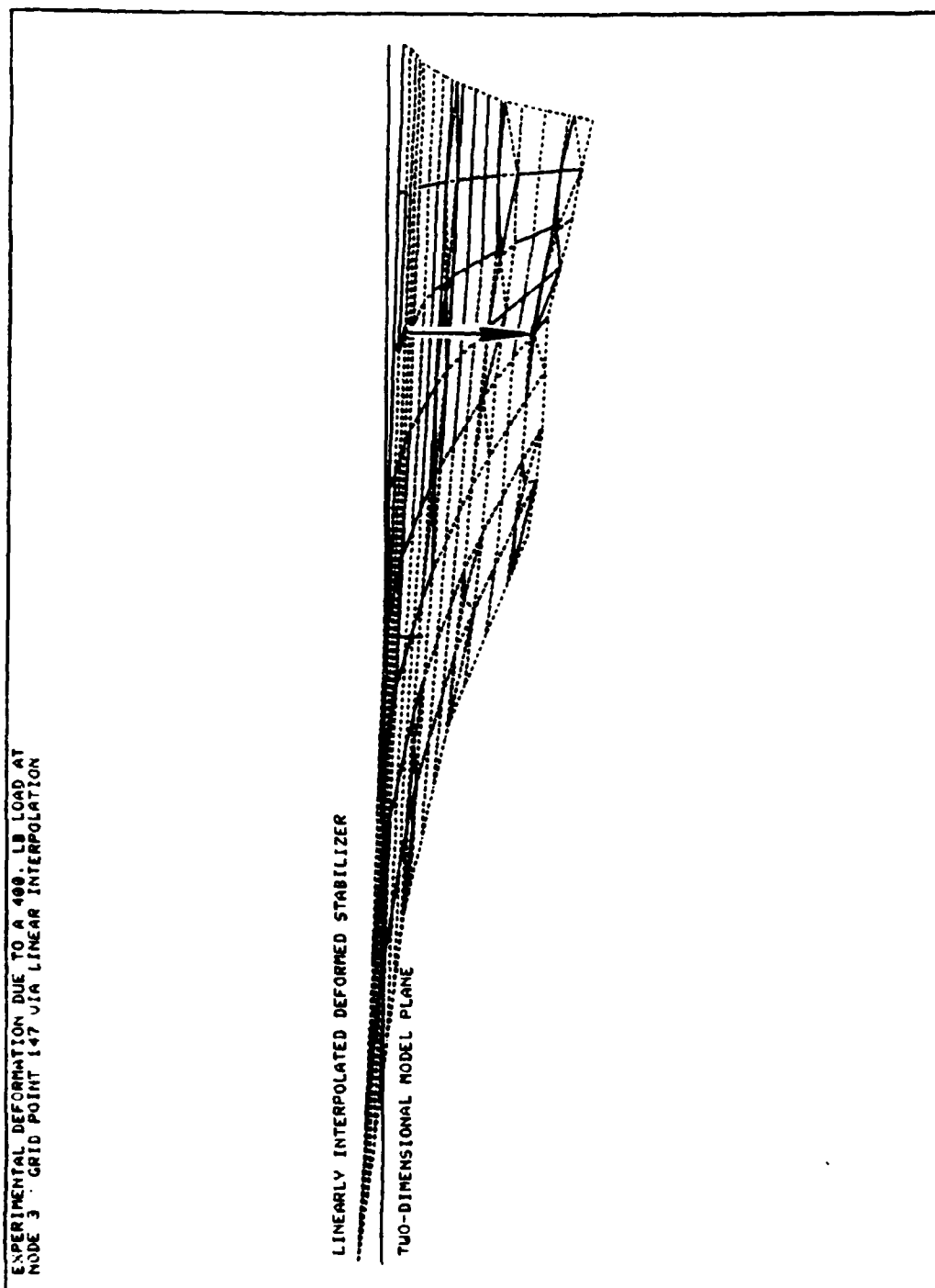


Figure B-1. Subcase 1 Experimental Deformation

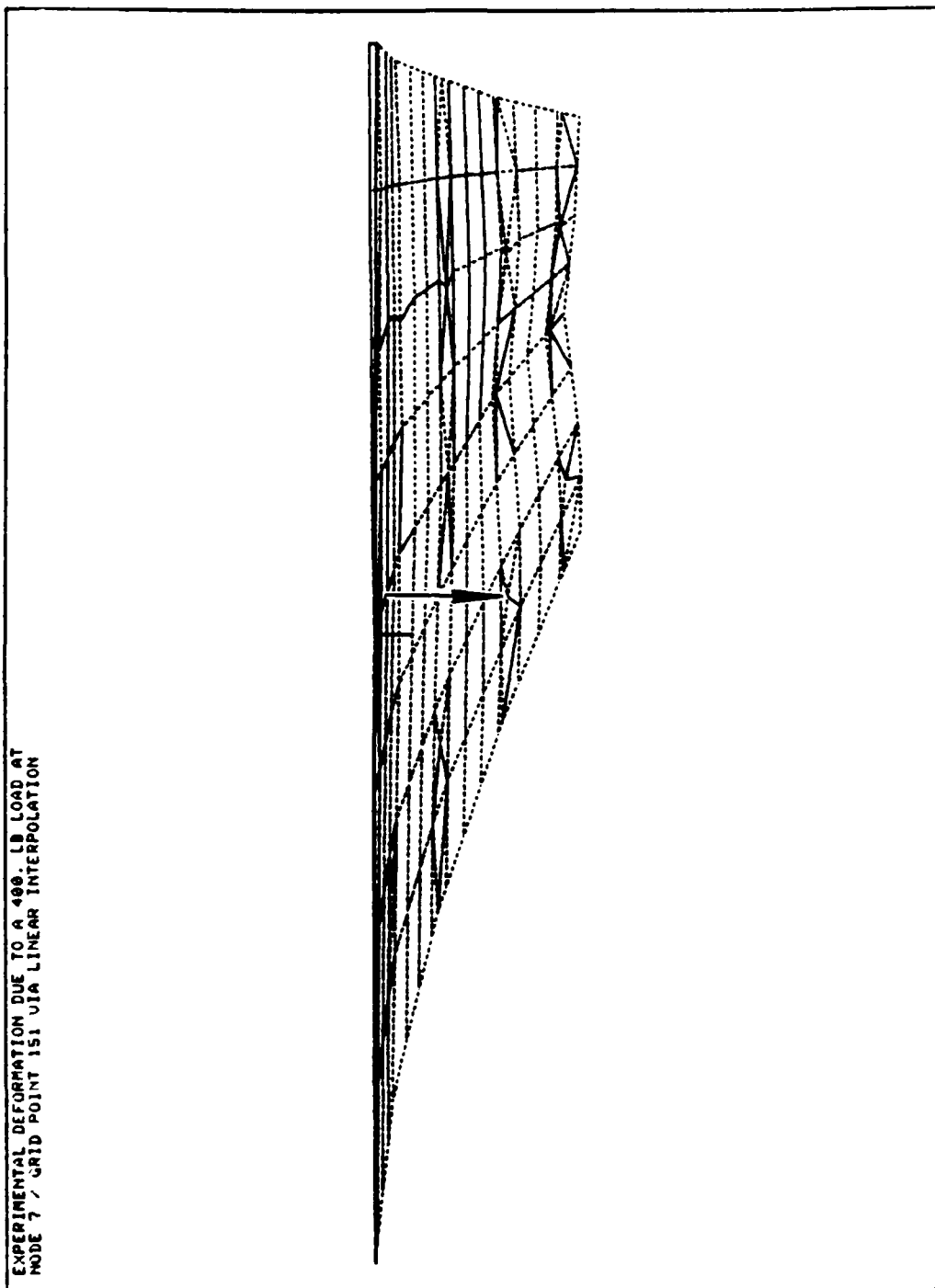


Figure B-2. Subcase 2 Experimental Deformation

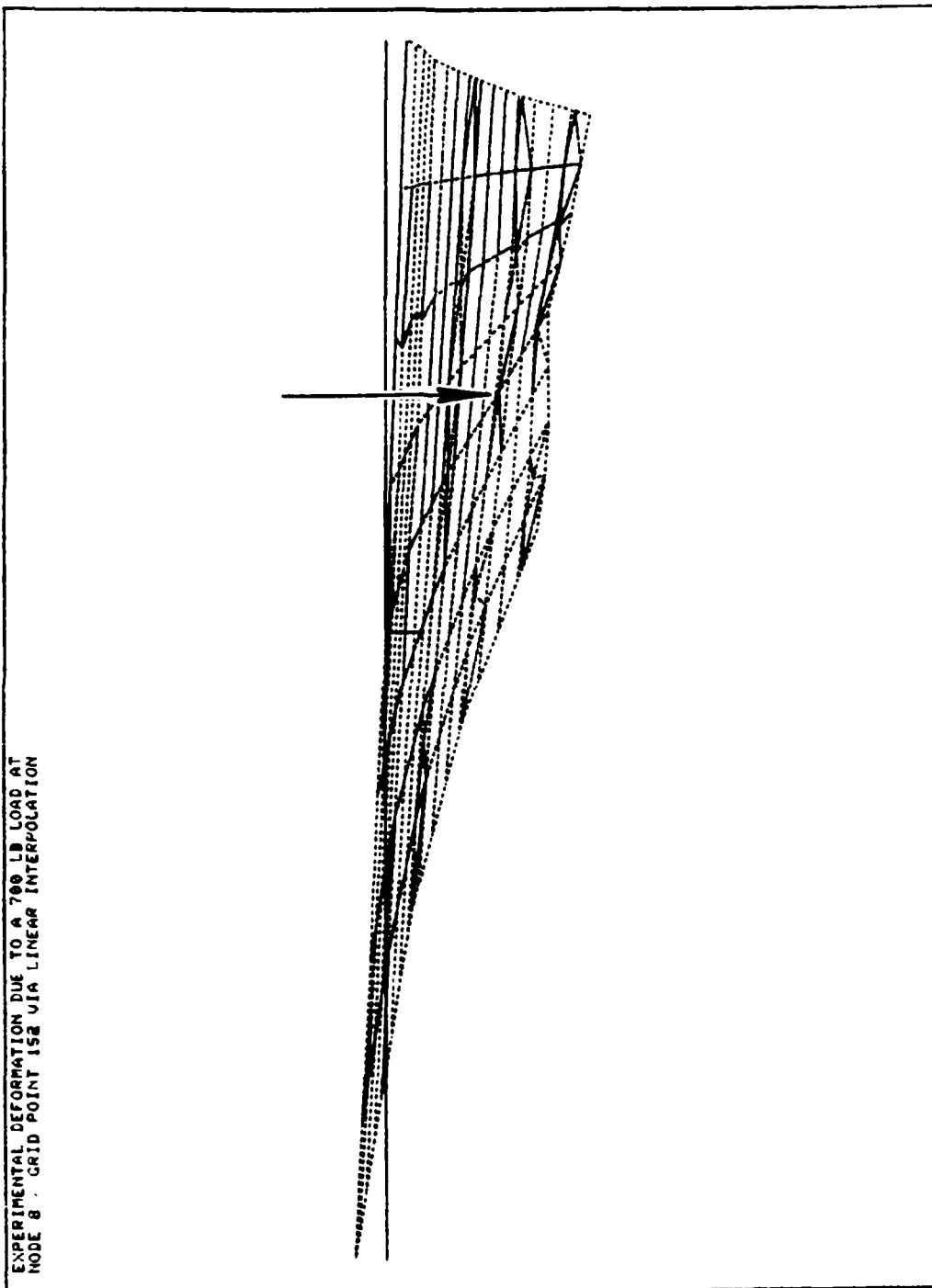


Figure B-3. Subcase 3 Experimental Deformation

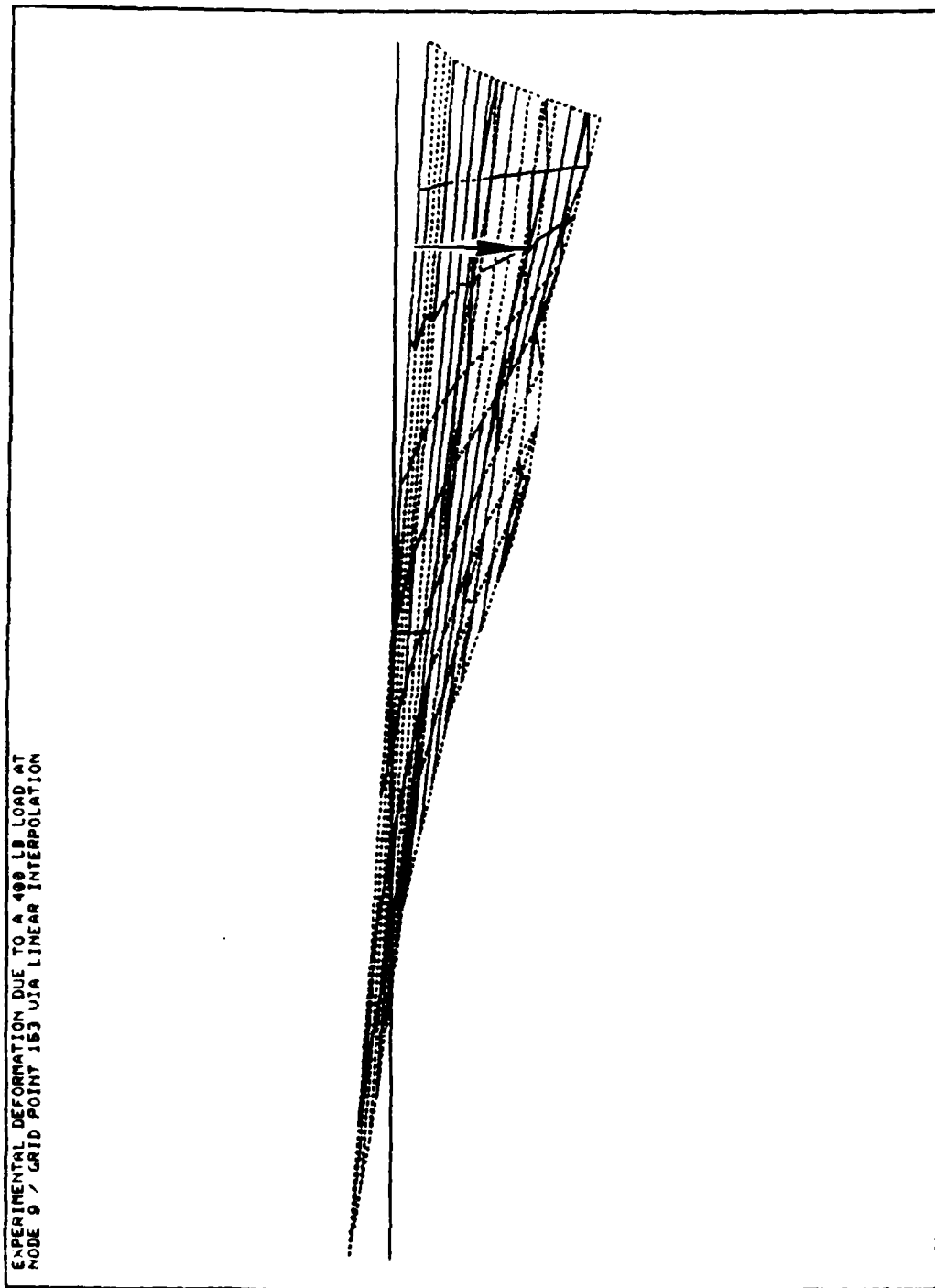


Figure B-4. Subcase 4 Experimental Deformation

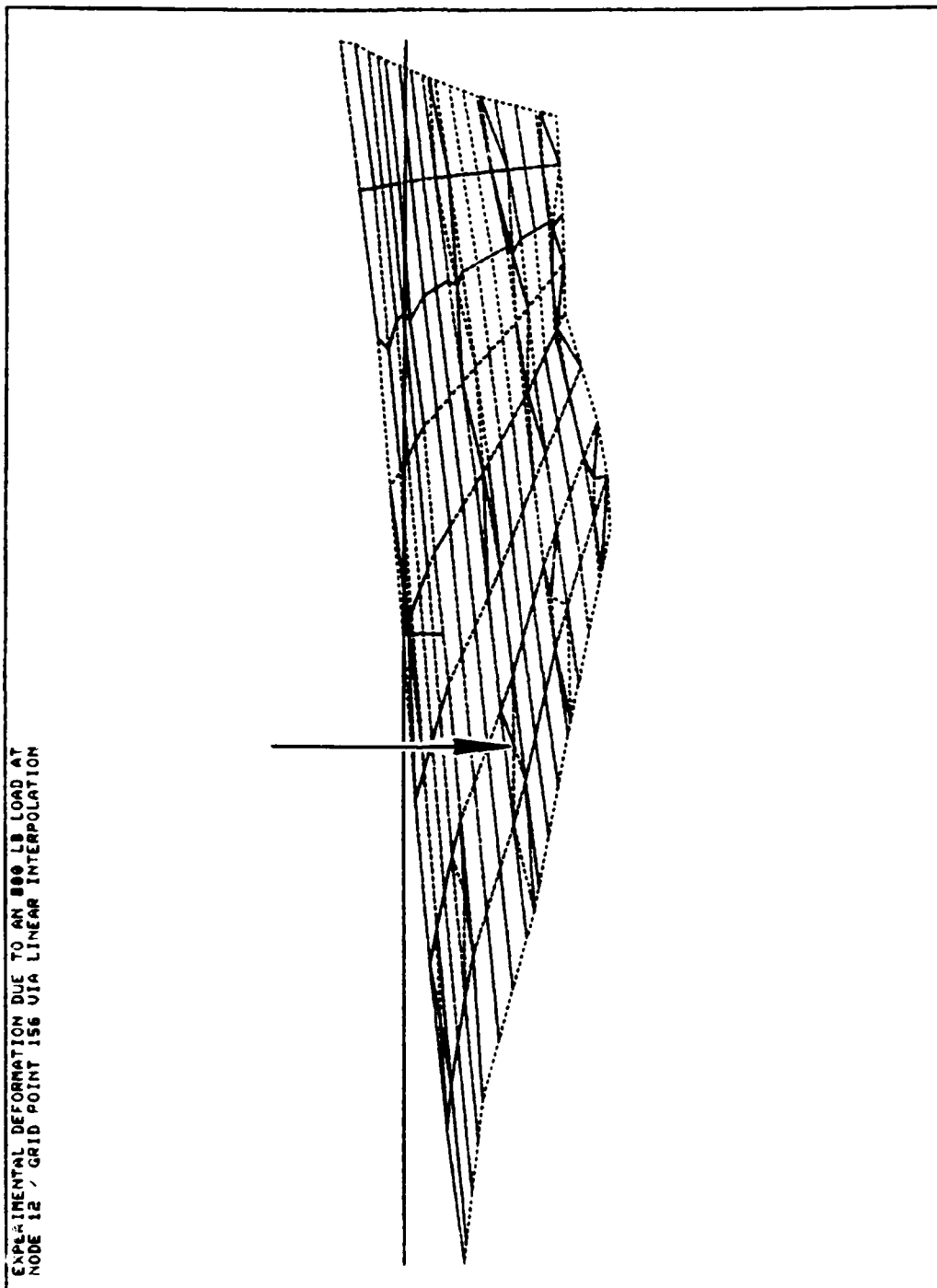


Figure B-5. Subcase 5 Experimental Deformation

EXPERIMENTAL DEFORMATION DUE TO A 1200 LB LOAD AT
NODE 13 / GRID POINT 157 VIA LINEAR INTERPOLATION

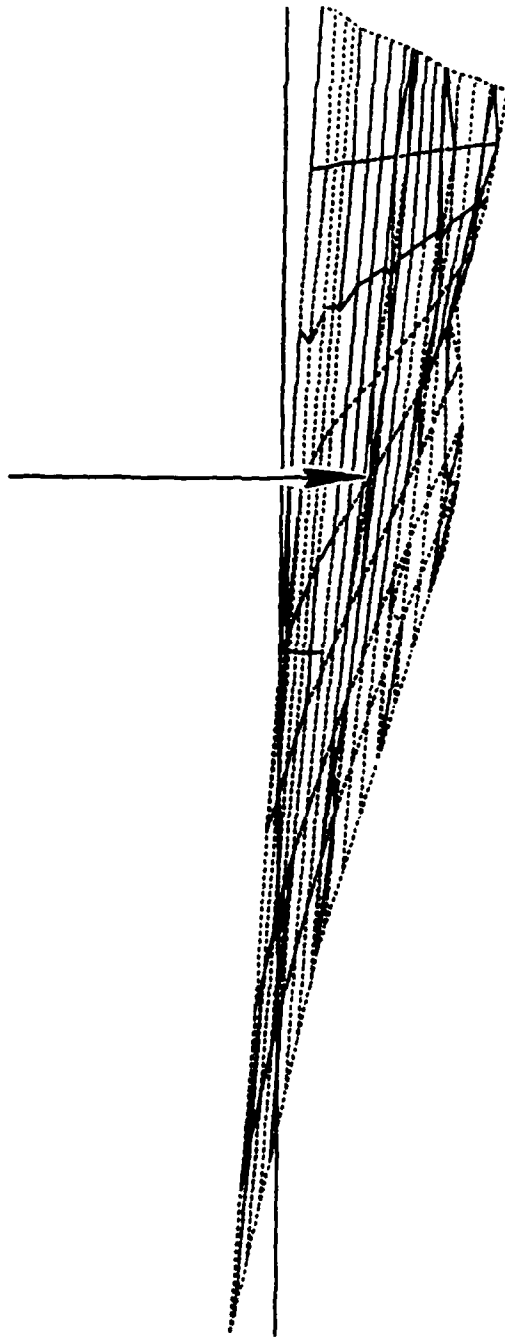


Figure B-6. Subcase 6 Experimental Deformation

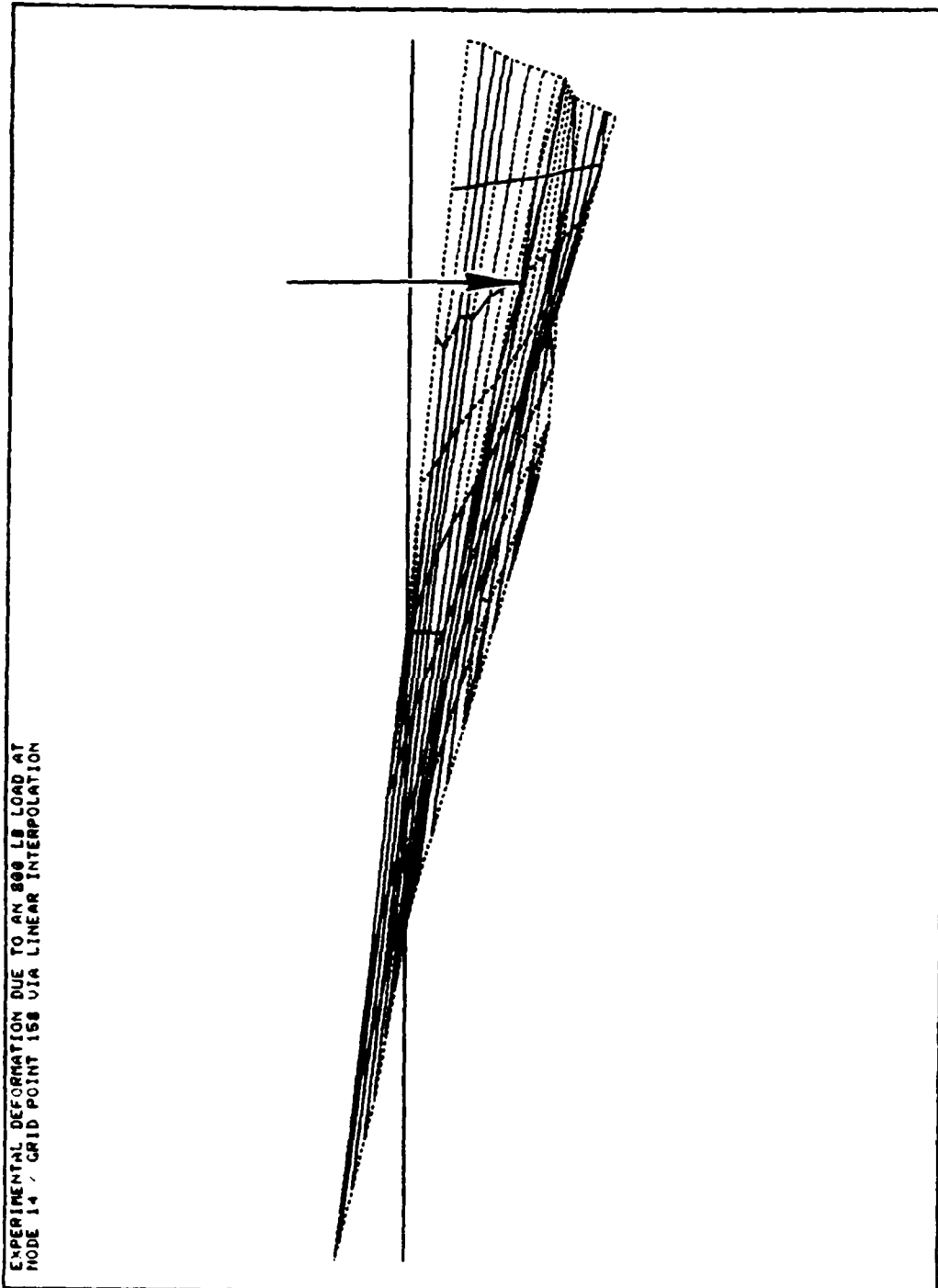


Figure B-7. Subcase 7 Experimental Deformation

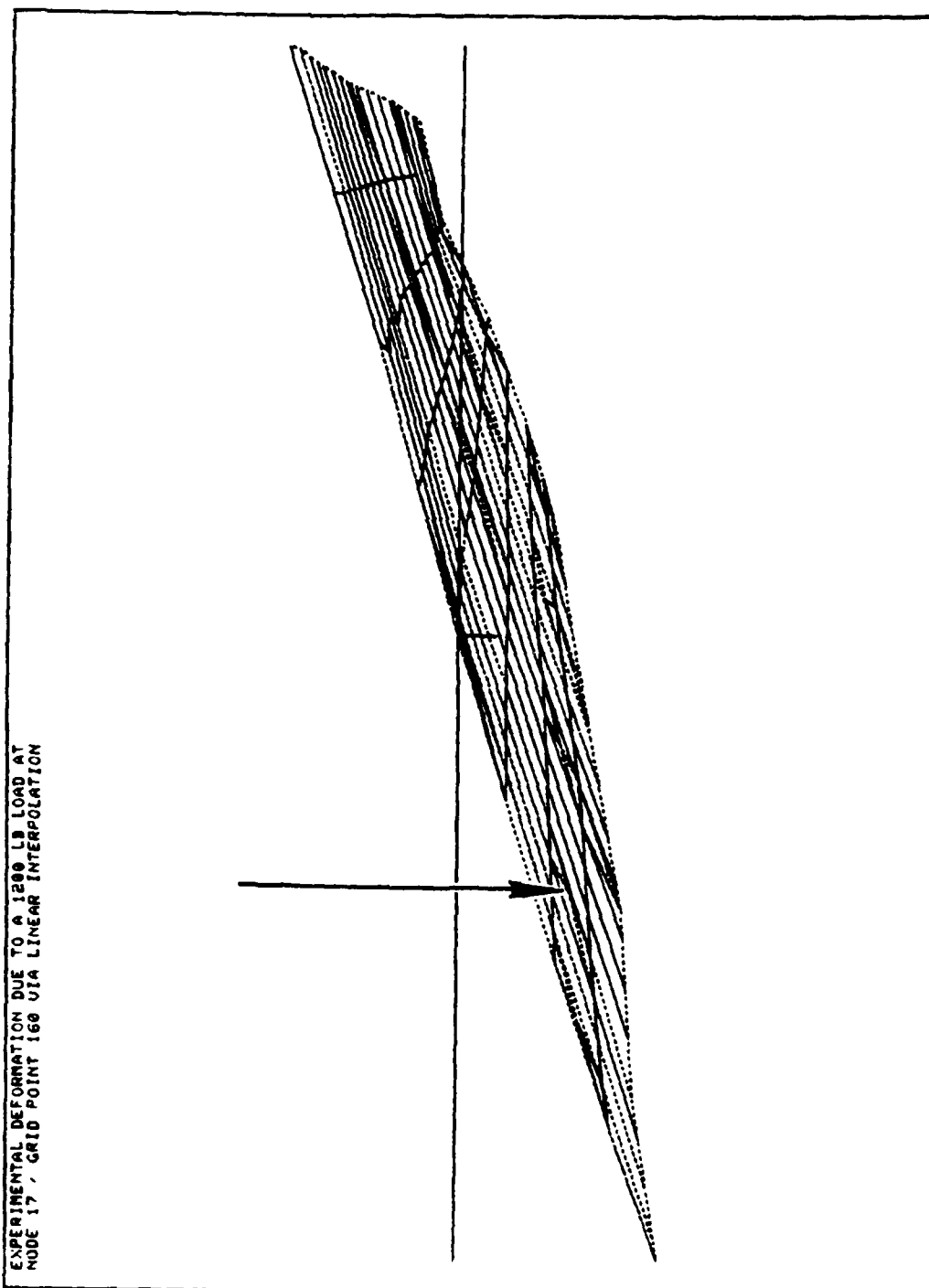


Figure B-8. Subcase 8 Experimental Deformation

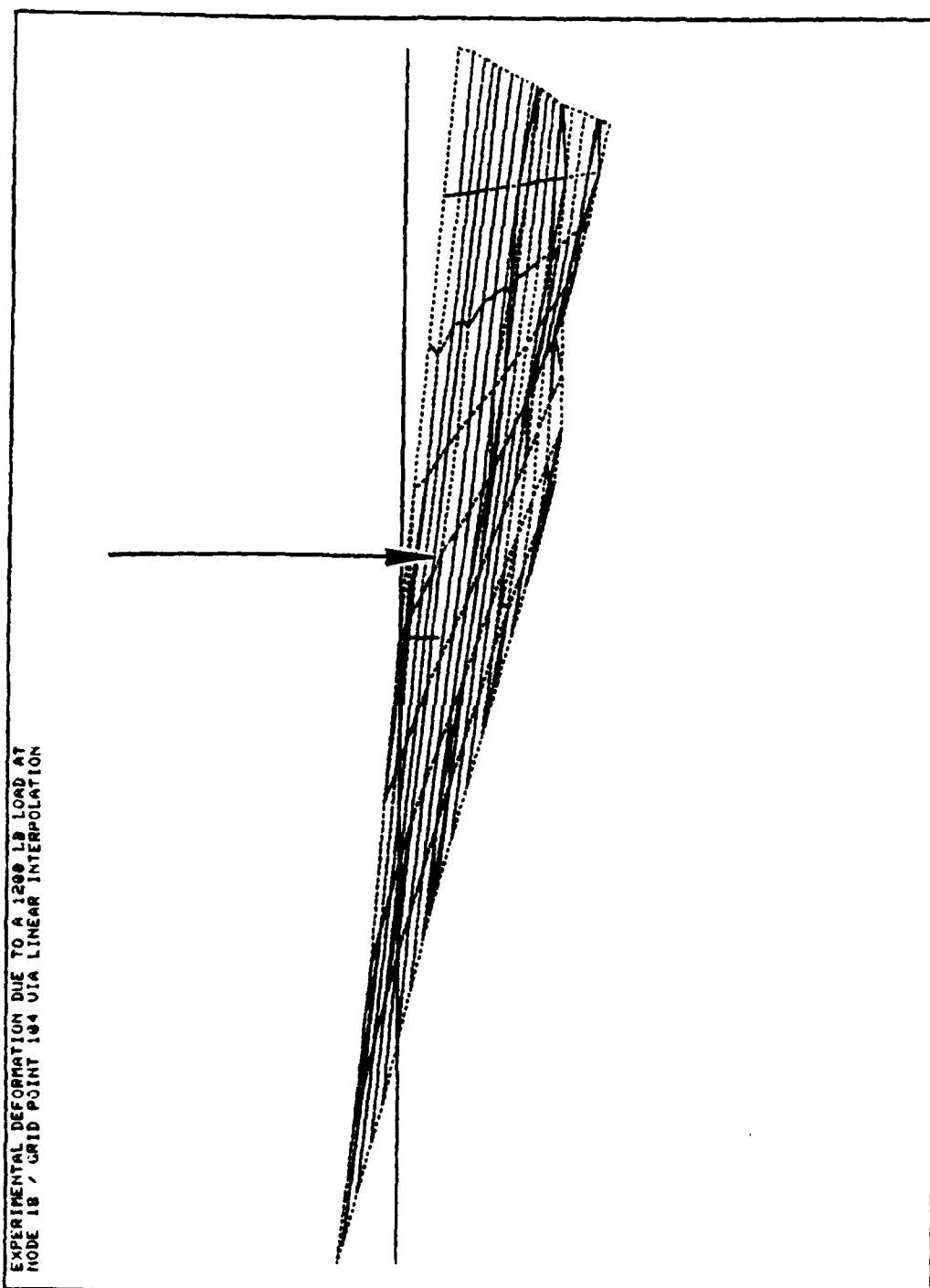


Figure B-9. Subcase 9 Experimental Deformation

EXPERIMENTAL DEFORMATION DUE TO A 1200 LB LOAD AT
NODE 19 / GRID POINT 106 VIA LINEAR INTERPOLATION

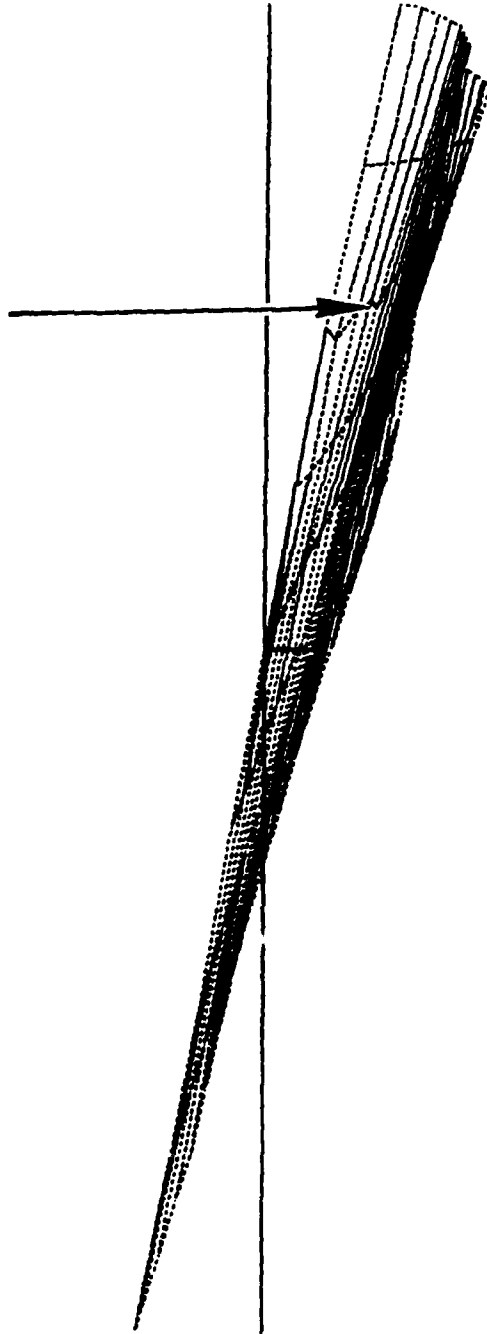


Figure B-10. Subcase 10 Experimental Deformation

Appendix C

Data Generator FORTRAN Program Summary

As mentioned in the text, a separate FORTRAN program (BDATA) was used to generate much of the FEM. The program had been authored by the thesis advisor (Capt H.C. Briggs). It had also been modified extensively during its usage by subsequent thesis students, Lassiter and Thomson. The program generated the cards defining the physical properties of the stabilator based on information contained in Northrop Reports (Ref 4 and 9) and Air Force Documents (Ref 10) for use in the Bulk Data Deck. Separate algorithms were used in forming modules to compute or write specific segments for output.

The modules (or sections) used in the program in order of occurrence can be described as follows:

- Module 1 - Input of data arrays for dimensions and function statements for other algorithms.

- Module 2 - User decision parameters for type of output (card-punch, hard copy-print, or tape), type stabilator mesh (Series 3, influence coefficient), size mesh (number of elements chordwise and spanwise), and variables used for refining displacement (torsion, thickness, and bending).

- Module 3 - Grid point mesh and coordinates are calculated

for following algorithms. Root rib coordinates are found from interpolation which accounts for the fuselage moldline. The influence coefficient nodes are not calculated, but specific values established in data tables.

- Module 4 - Grid points are sequenced for CQUAD1 elements with CTRIAL elements replacing those necessary to construct the influence coefficient model. Connectivity and property cards are developed for CQUAD1 and CTRIAL elements.
- Module 5 - Grid point connectivity for CBAR elements for the main spar and associated property cards. These are explicit for the influence coefficient model.
- Module 6 - Generate CBAR elements for the tip rib, connectivity, and associated property cards.
- Module 7 - Generate CBAR elements for the leading edge extrusion, connectivity, and associated property cards.
- Module 8 - Generate CBAR elements for the auxiliary spar, connectivity, and associated property cards.
- Module 9 - Generate elements for the ribs on Series 2 only stabilator (not used herein, for Series 3 analysis).
- Module 10 - Generate CBAR elements for the root rib, connectivity, and associated property cards.

- Module 11 - Connectivity and property cards for the torque tube are output explicitly based on model chosen (influence coefficient versus variable size mesh).
- Module 12 - Generate CBAR elements for trailing edge closure, connectivity, and associated property cards.
- Module 13 - Output coordinate system cards. Two rectangular systems are used, the global system and a system embedded in the planform of the stabilator (CORD2R).
- Module 14 - Output GRID cards. Influence coefficient model grid points are moved or generated as necessary, based on fixed mesh size.
- Module 15 - Output MAT1 and MAT2 material property cards. These are explicit except for variations allowed in determining properties for the orthotropic material.
- Module 16 - Subroutine for interpolation used in above algorithms.
- Module 17 - Subroutine for development of property card specifics used in above algorithms.
- Module 18 - Subroutine for output of formatted data used in above algorithms.

Although many modules were used in the generation of the data, the program modular format was of a great benefit during analysis for creating Bulk Data Decks with varying parameters. The program was modified for this analysis to include the generation of those elements, connectivities, and grid points relevant to the generation of the influence coefficient model. The influence model was developed for an 8 element chordwise by 15 element spanwise mesh. In reviewing the contents of the program, a significant error in calculating the inertia of the membrane elements was discovered and corrected.

Appendix D

Grid Point Identifications

Expanded elemental sections from Figure 7, page 19, are presented in this appendix for better clarification of the relative locations of the various elements used in developing the FEM. In all views, the tip is located at the top and forward is to the left.

SERIES 3 INF CO MODEL
GRID POINTS FOR MSS 77.36 TO 85.00

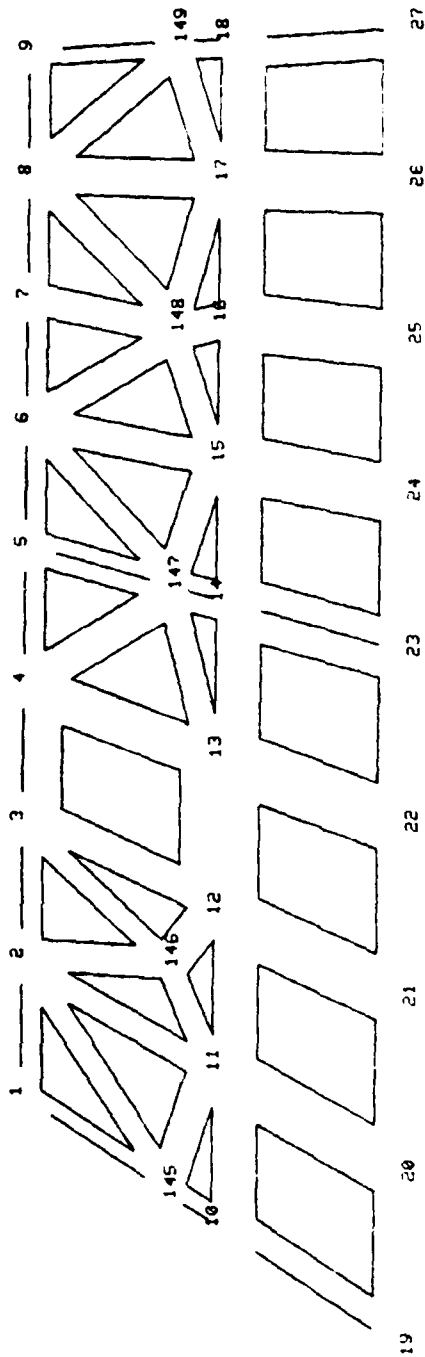


Figure D-1. Grid Point Identification GP 1 to GP 27

SERIES 3 INF CO MODEL
GRID POINTS FOR HSS 62.00 TO 77.36

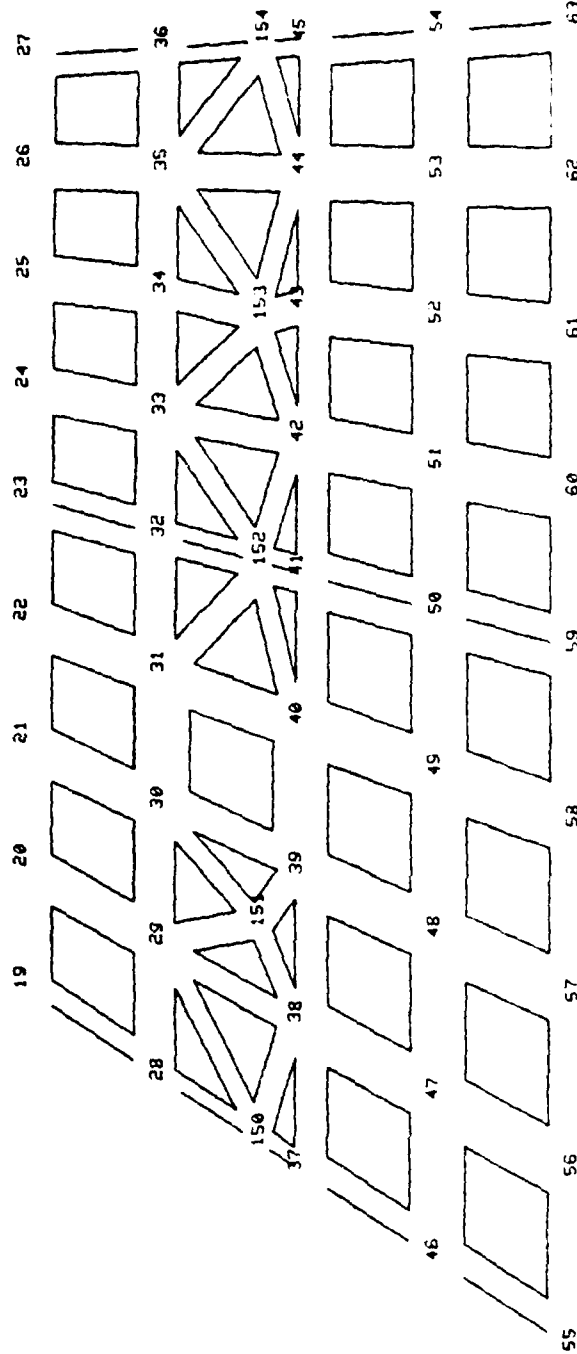


Figure D-2. Grid Point Identification GP 19 to GP 63

SERIES 3 INF CO MODEL
GRID POINTS FOR MSS 46.80 TO 62.08

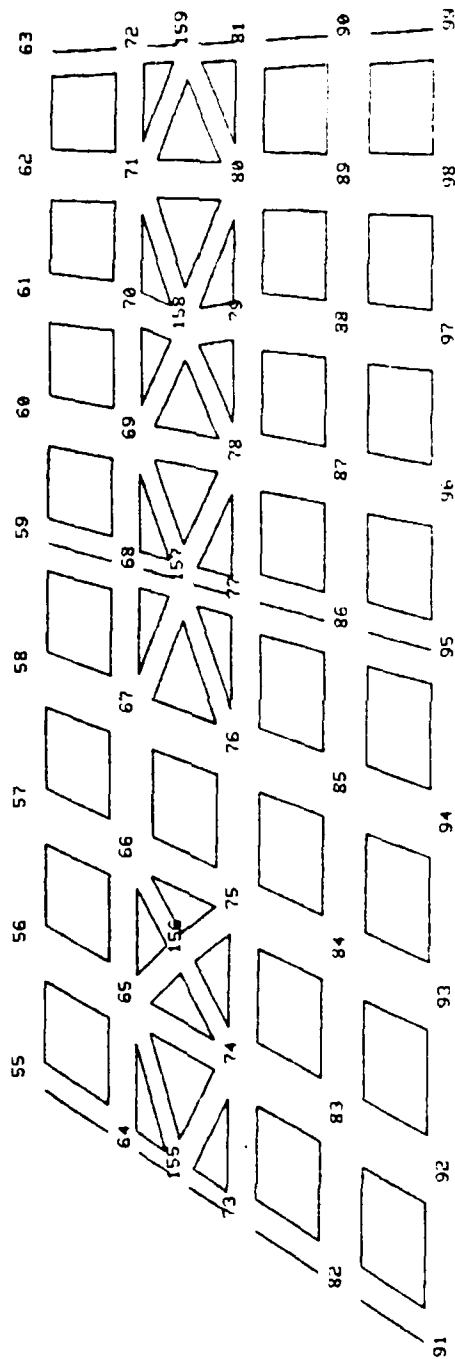


Figure D-3. Grid Point Identification CP 55 to CP 99

SERIES 3 INF CO MODEL
GRID POINTS FOR MSS 35.14 TO 46.80

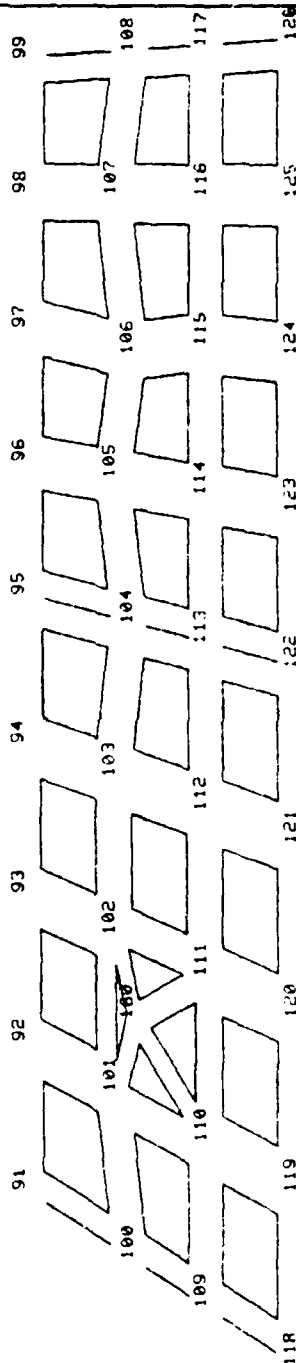
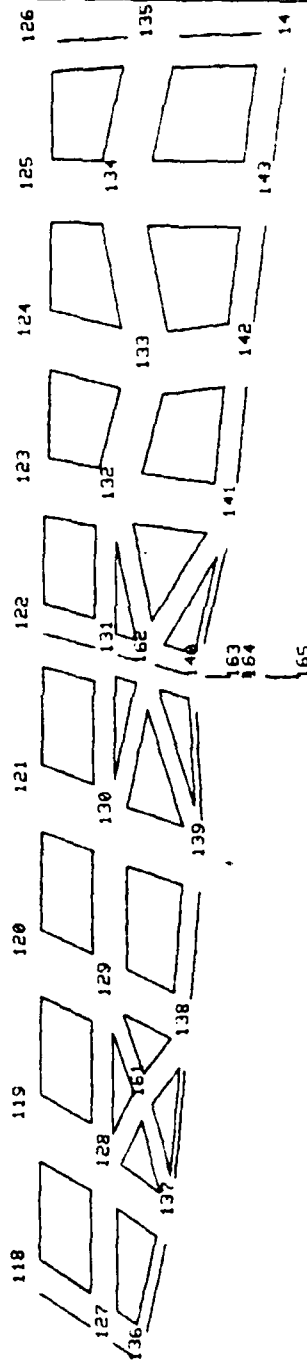


Figure D-4. Grid Point Identification GP 91 to GP 126

SERIES 3 INF CO MODEL
GRID POINTS FOR HSS 22.64 TO 35.34



NOTE: Grid Point 166 at HSS 0.00

Figure D-5. Grid point Identification CP 118 to CP 166

Appendix E

Alter Routine for Error Value Calculation

NASTRAN Executive Control Deck Section

```
ID JO SAWDY
APP DISPLACEMENT
SOL 1
TIME 4
ALTER 134
PARTN UGV,,ROWPT / NAS,,, / C,N,1 $
ADD NAS,EXP / DIFF / C,Y,ALPHA=(1.0,0.0) / C,Y,BETA=(-1.0,0.0) $
TRNSP DIFF / DIFT $
MPYAD DIFT,DIFF, / DSQ / C,N,D $
DIAGONAL DSQ / ERROR / C,Y,OPT=COLUMN / V,Y,POWER=.5 $
MPYAD SUMCOL,ERROR, / ERRSUM / C,N,O $
MATPRN NAS,EXP,DSQ,ERROR,ERRSUM // $
ENDALTER
CEND
```

The above Executive Control Deck section was used in formulating the scalar error value in NASTRAN. After the solution of displacements for all subcases is computed, the program was altered (after step 134) to extract (PARTN) the twenty-five data points for each subcase from the solution set (UGV) using a column matrix of ones and zeros (ROWPT). Using the ADD operation, the experimental

displacements (EXP) are subtracted from the appropriate NASTRAN computed displacements (NAS) to form a matrix of difference in displacements (DIFF). The transpose (TRNSP) of DIFF is formed as DIFT. The product of DIFT and DIFF matrices then forms the sum of the squares (DSQ). The square root of the diagonal terms was formed into a column vector (ERROR) representing the error value for each of the subcases. Using the operator multiply and add (MPYAD), the subcase error values (ERROR) were summed using a row vector (SUMCOL) to form the overall scalar error value (ERRSUM). This value represented the sum of the differences in displacement for 250 data points compared.

Appendix F

Two-Dimensional Model Versus Torsion-Cell

Inasmuch as the two-dimensional model is made of solid elements, it is deficient the mechanism for modelling torsion-cell shear flow contribution to the stiffness of the airfoil. A psuedo-torsional mechanism can be introduced to the FEM by considering the plates as orthotropic elements instead of isotropic elements (as was utilized in previous theses). The application of orthotropic elements for a unit span is investigated.

Allow the cross-section of the airfoil to be approximated by a diamond shape of height h_a and chord width C with a constant skin thickness of t_a as shown.

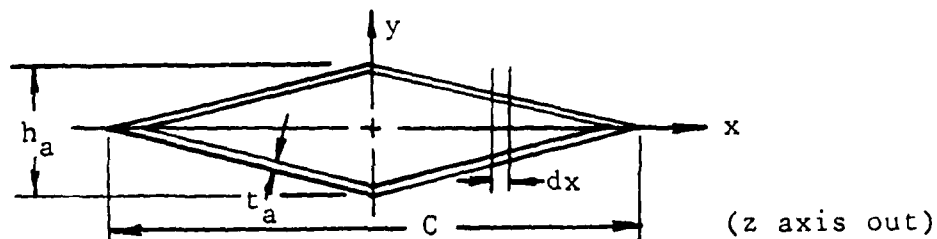


Figure F-1. Diamond Shape Approximation of Airfoil

The two-dimensional model is similarly approximated by a thin rectangular shape of height t_p and chord width C .

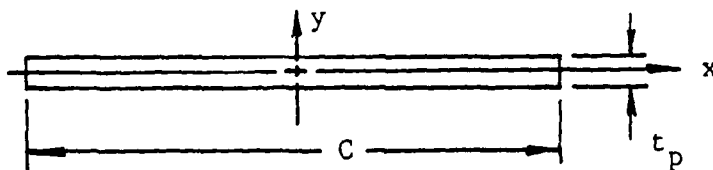


Figure F-2. Thin Rectangular Shape Approximation for FEM

It is desired to construct the EI and GJ products of the thin rectangular plate such that they are equivalent to those of the diamond shaped airfoil. The EI_a product of the airfoil surface plates about the x axis can be approximated by

$$EI_a = 4E \int_0^{C/2} \frac{t_a (h_a(x))^2 dx}{4} \quad (\text{Ref 11})$$

$$\text{where } h_a(x) = \frac{-h_a}{C} x + \frac{h_a}{2} \quad (0 \leq x \leq C/2)$$

Substituting the equation for the skin surface geometry, the EI_a product can be reduced to

$$EI_a = E \left(\frac{t_a h_a^2 C}{24} \right)$$

Similarly, the EI_p product for the thin rectangular shape about the x axis can be expressed by

$$EI_p = E \left(\frac{t_p^3 C}{12} \right) \quad (\text{Ref 12})$$

For a constant E, an equivalent thickness can be found from equating EI_a and EI_p .

$$t_p = \sqrt[3]{\frac{t_a h_a^2}{2}}$$

Thus, the thickness of the thin rectangular shape is a function of the skin thickness and airfoil height. This relationship is used in developing a consistent torsional moment of

inertia for $G_a J_a$ and $G_p J_p$ products about the z axis. The airfoil $G_a J_a$ product can be expressed by

$$G_a J_a = G_a \frac{4A^2}{\int \frac{ds}{t_a}} \quad \begin{array}{l} \text{(s is airfoil perimeter)} \\ \text{(Ref 11)} \end{array}$$

Substituting for the airfoil area and perimeter,

$$G_a J_a = G_a \left\{ \frac{4 \left(C \frac{h_a}{2} \right)^2 t_a}{4 \left[\left(\frac{h_a}{2} \right)^2 + \left(\frac{C}{2} \right)^2 \right]^{\frac{1}{2}}} \right\}$$

Then for $h_a \ll C$, the product $G_a J_a$ reduces to

$$G_a J_a = \left(\frac{G_a h_a^2 C t_a}{2} \right)$$

The $G_p J_p$ product for a thin rectangular plate can be expressed by

$$G_p J_p = G_p \left(\frac{C t_p^3}{3} \right) \quad \text{(Ref 12)}$$

Substituting for t_p in terms of the airfoil parameters and equating $G_a J_a$ to $G_p J_p$, an equivalent G relationship can be developed.

$$G_p = 3 G_a$$

Thus, the plate shear modulus requires three times the

the airfoil shear modulus value for an equivalent thickness FEM. The two-dimensional model did not use G (shear modulus) for the plate elements. Therefore, Young's modulus (E) was varied for changes in bending. However, varying E for an isotropic plate would result in bending changes for both directions of the planform. Thus, it became imperative to segregate the two directions of bending for the two-dimensional FEM. Orthotropic plates allowed the selection of two separate E values for optimizing the planform deformation.

Appendix G

Graphic Presentation of NASTRAN Analytical Results

The views presented were developed using the output of the NASTRAN analytical displacements for all (166) grid points as input to the graphics code GCSNAST. The orientation of the view is the same as that in Appendix B to facilitate visual comparisons. As in Appendix B, the view is the same as the experimental tests set-up (shown in Figs 2 and 3). The two-dimensional FEM forms a reference plane (horizontal line) for the undeformed stabilator. The leading edge is to the left and the trailing edge is to the right.

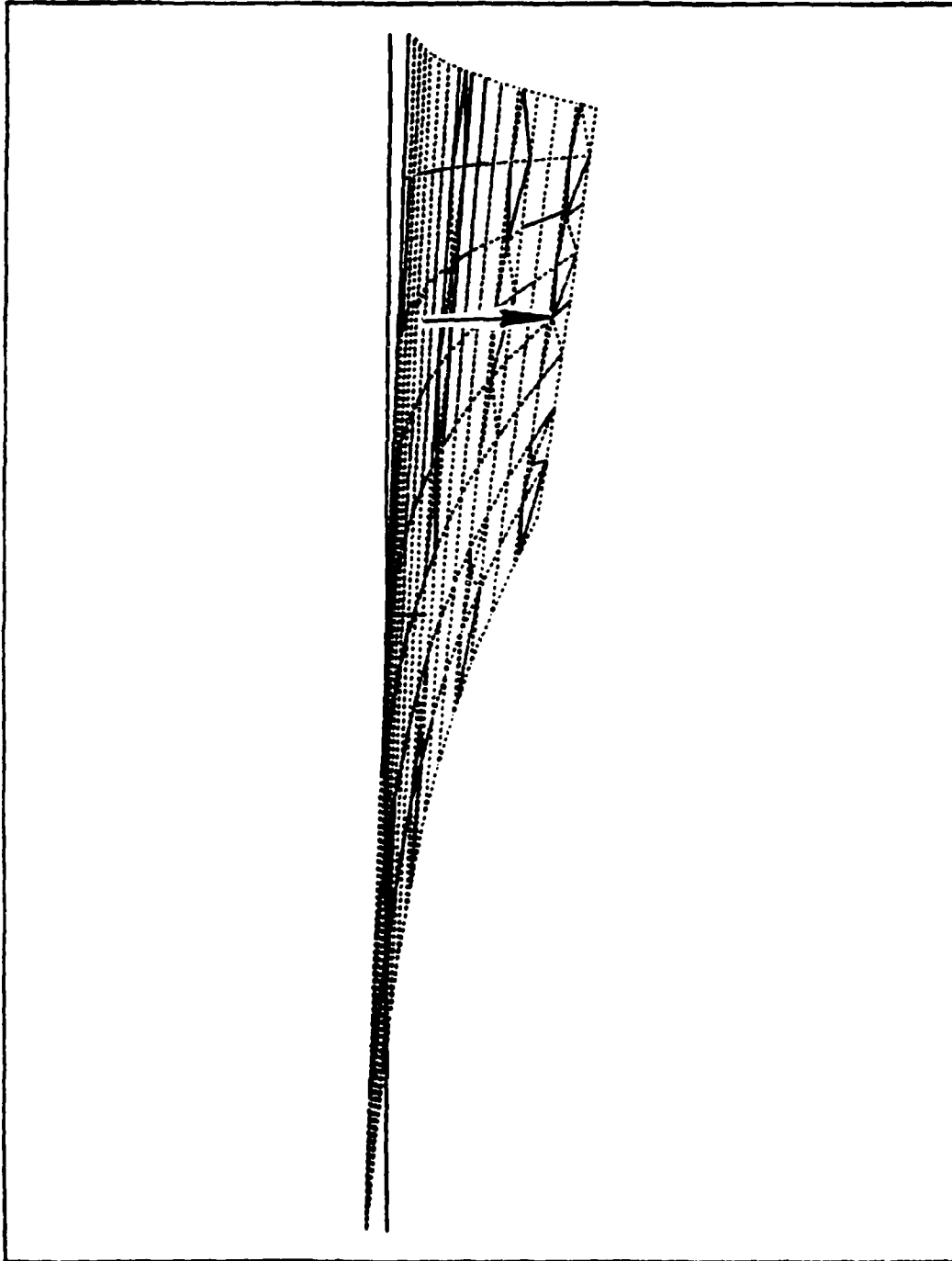


Figure G-1. Subcase 1 NASTRAN Analytical Deformation Due to
a 382 lb Load at GP 147

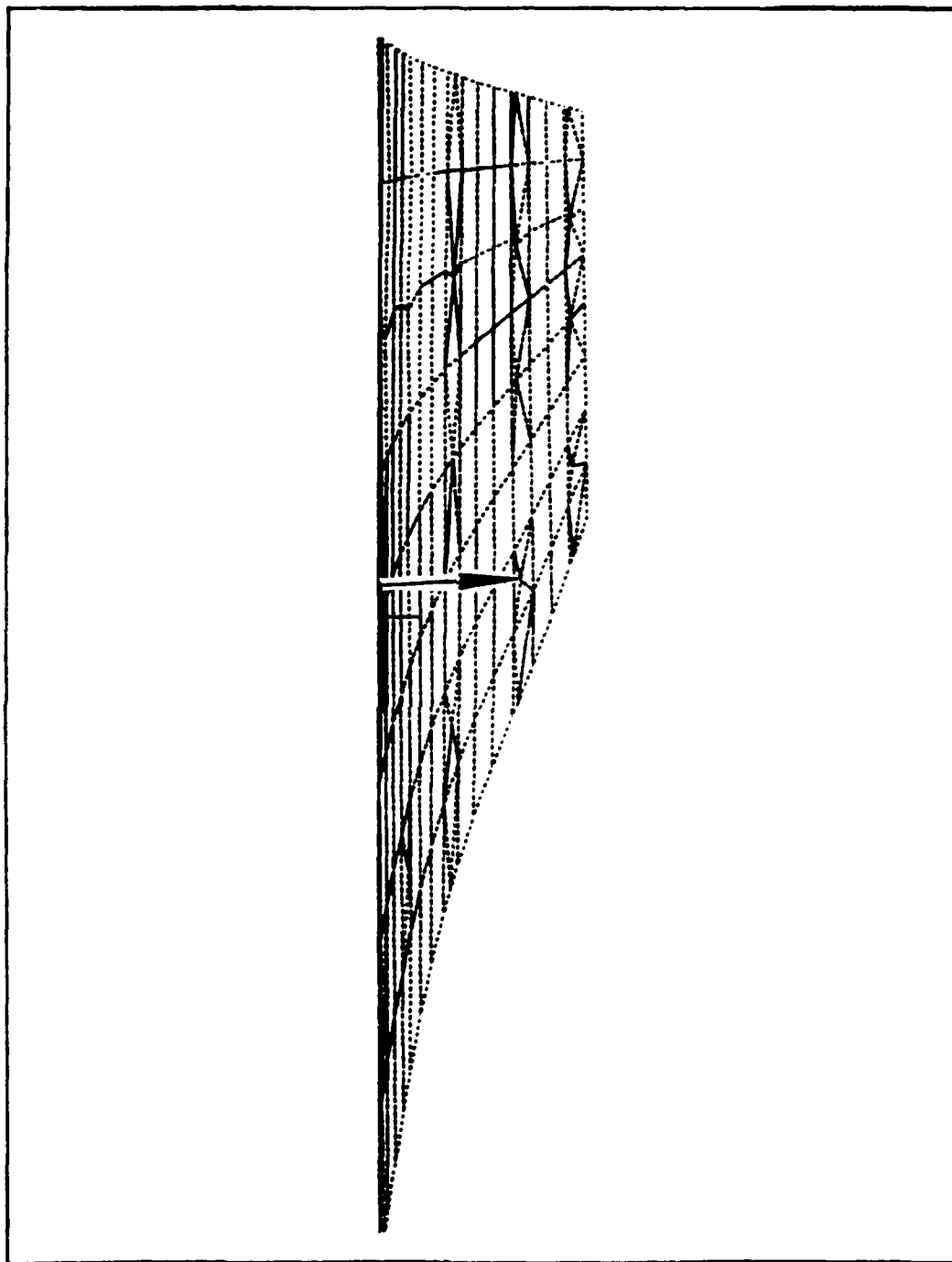


Figure C-2. Subcase 2 NASTRAN Analytical Deformation Due to
a 382 lb Load at CP 151

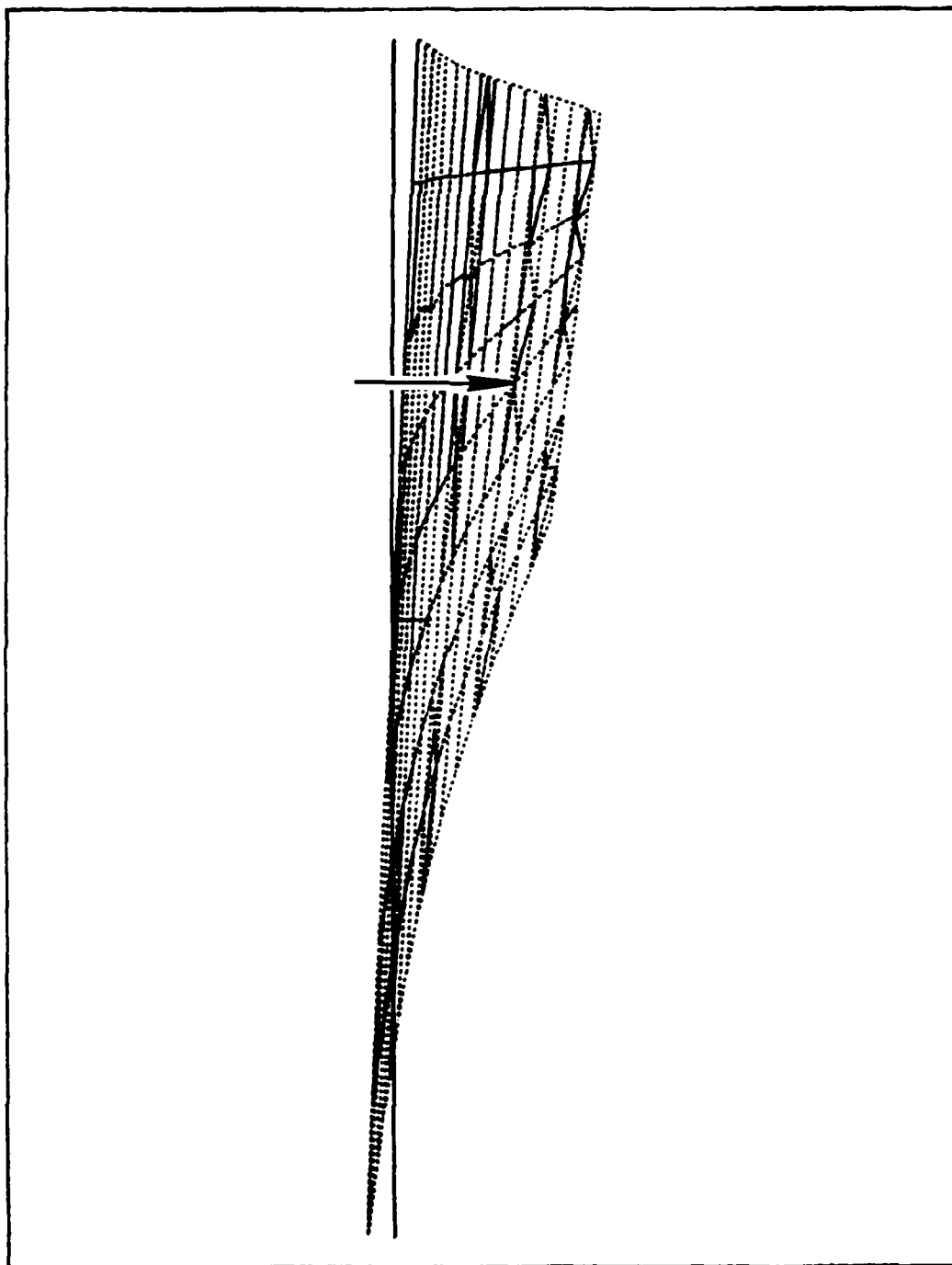


Figure G-3. Subcase 3 NASTRAN Analytical Deformation Due to
a 682 lb Load at CP 152

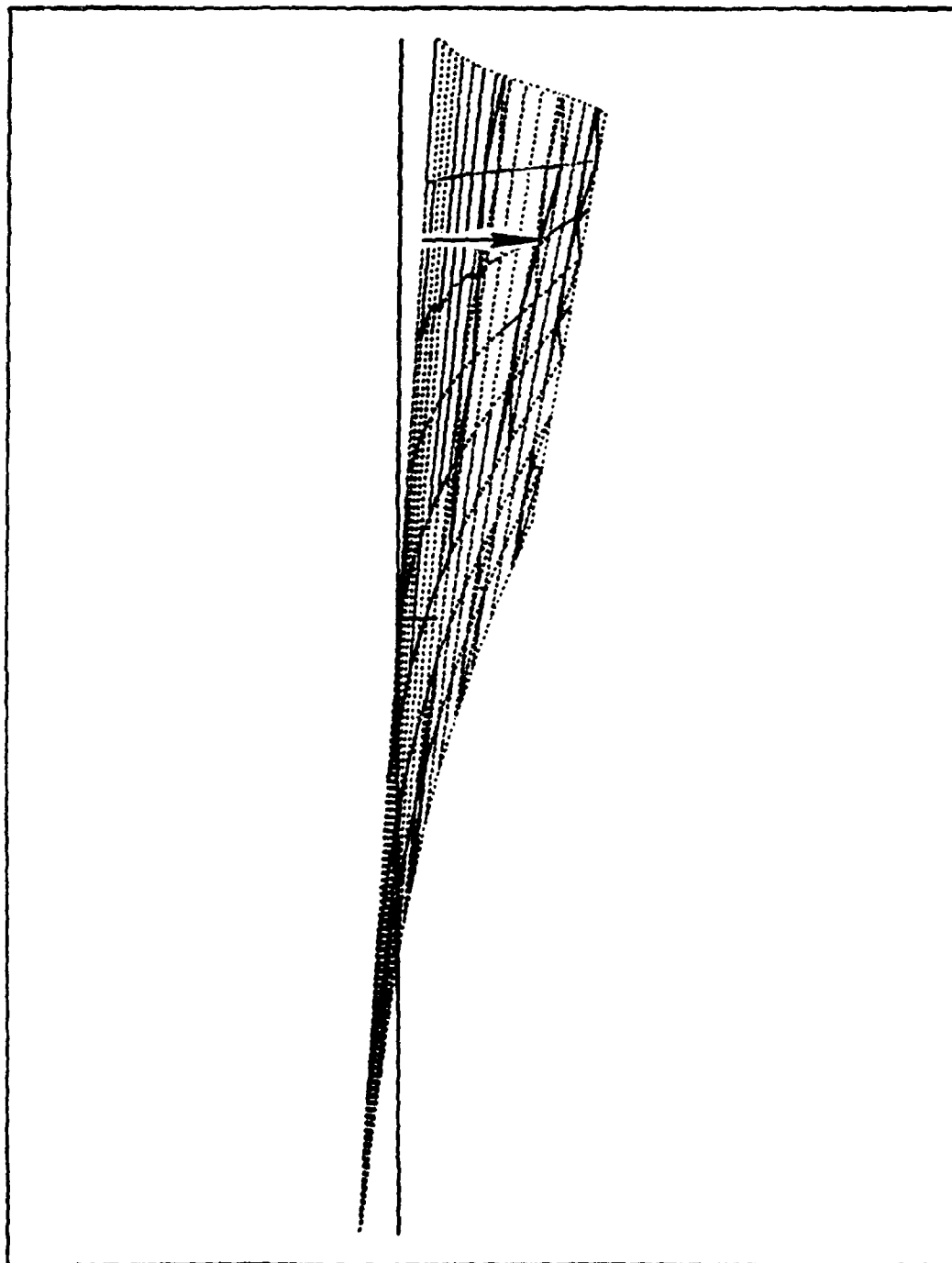


Figure C-4. Subcase 4 NASTRAN Analytical Deformation Due to
a 382 lb Load at CP 153

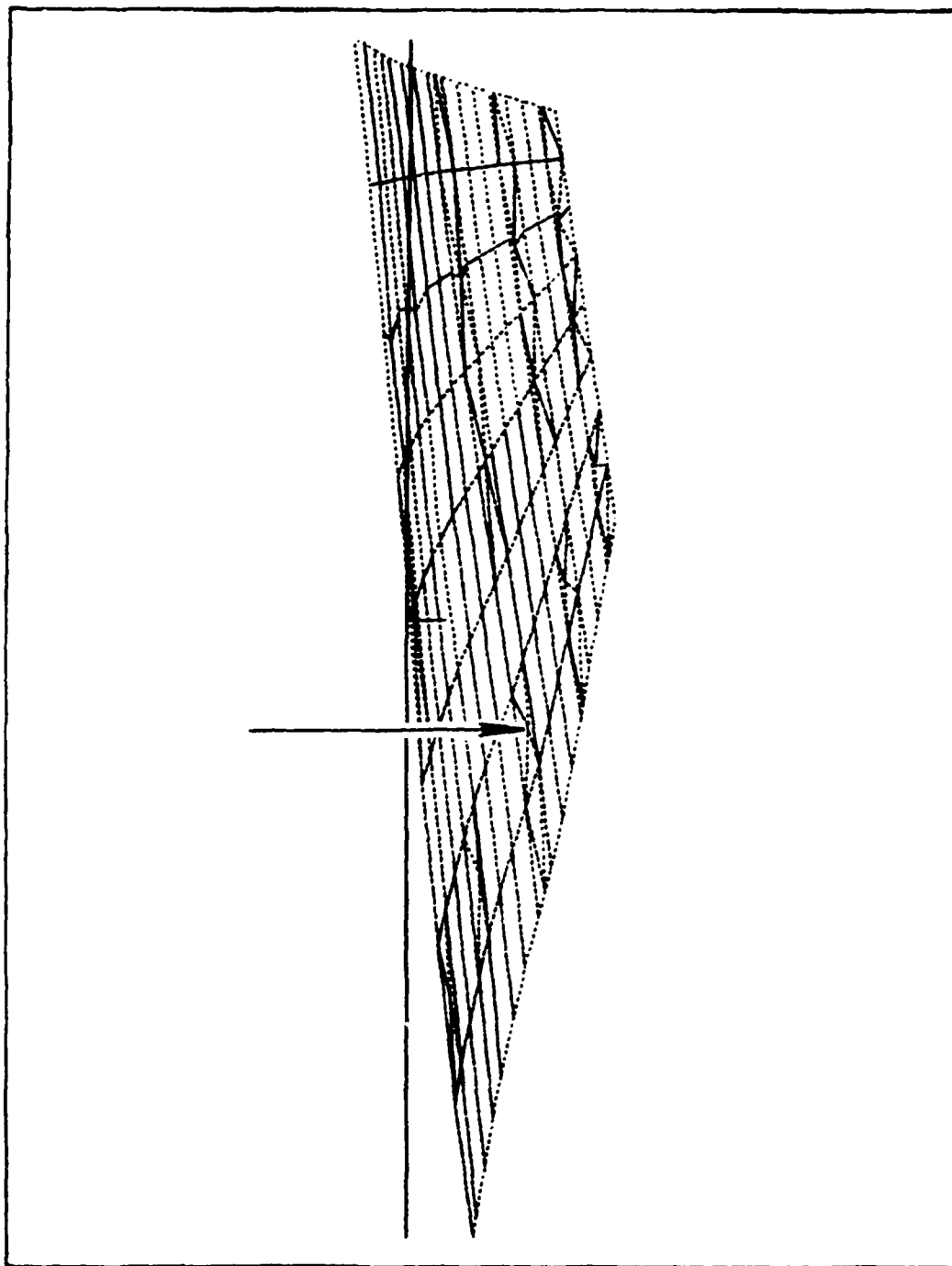


Figure C-5. Subcase 5 NASTRAN Analytical Deformation Due to
a 782 lb Load at CP 156

AD-A111 100

AIR FORCE INST OF TECH WRIGHT-PATTERSON AFB OH SCHOO--ETC F/8 1/1
INVESTIGATION OF A TWO-DIMENSIONAL MODEL FOR THE PREDICTION OF --ETC(U)
DEC 81 J O SANDY

UNCLASSIFIED

AFIT/8AE/AA/81D-27

NL

2 of 2
SE
017-100



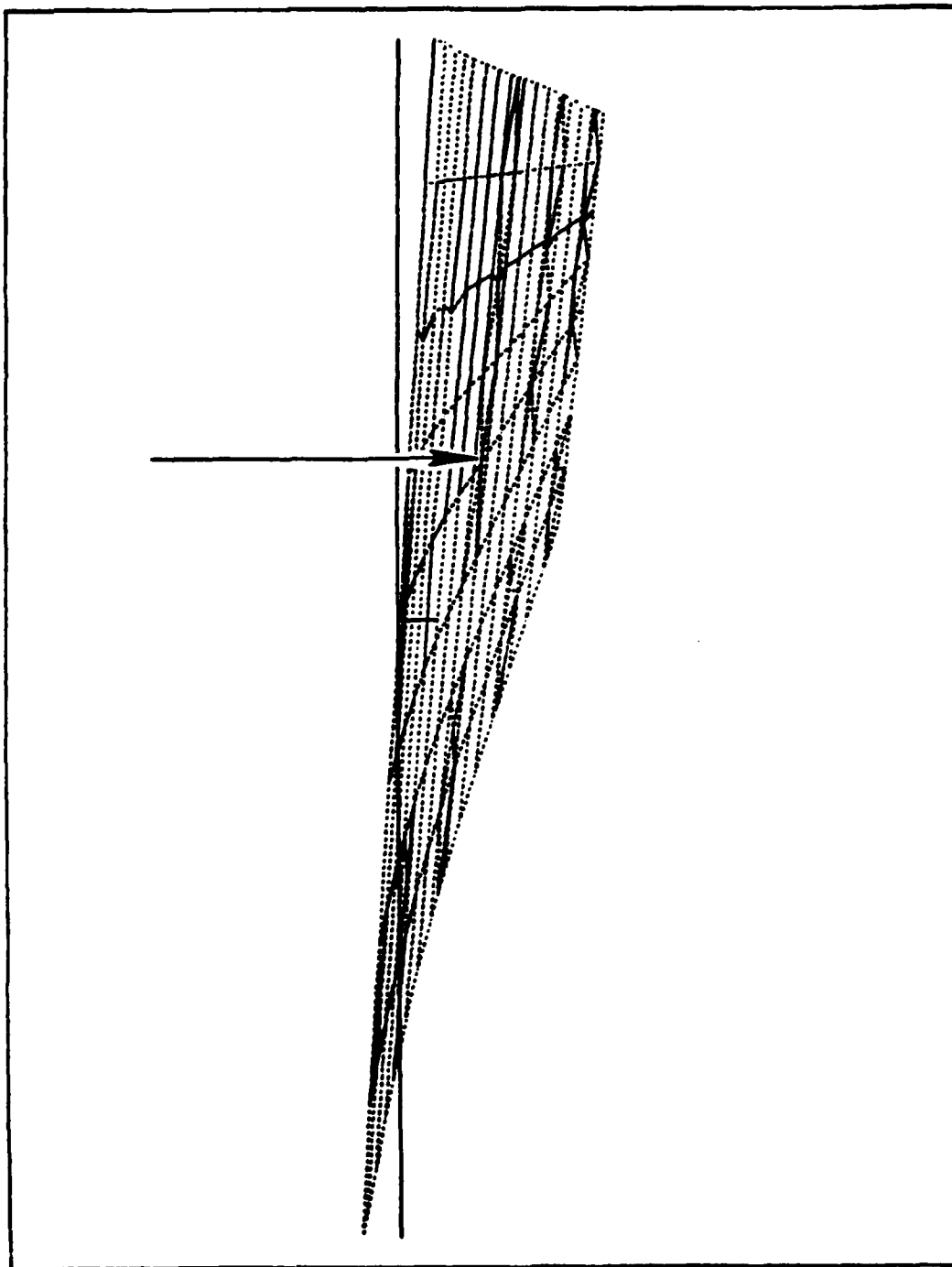


Figure G-6. Subcase 6 NASTRAN Analytical Deformation Due to
a 1182 lb Load at GP 157

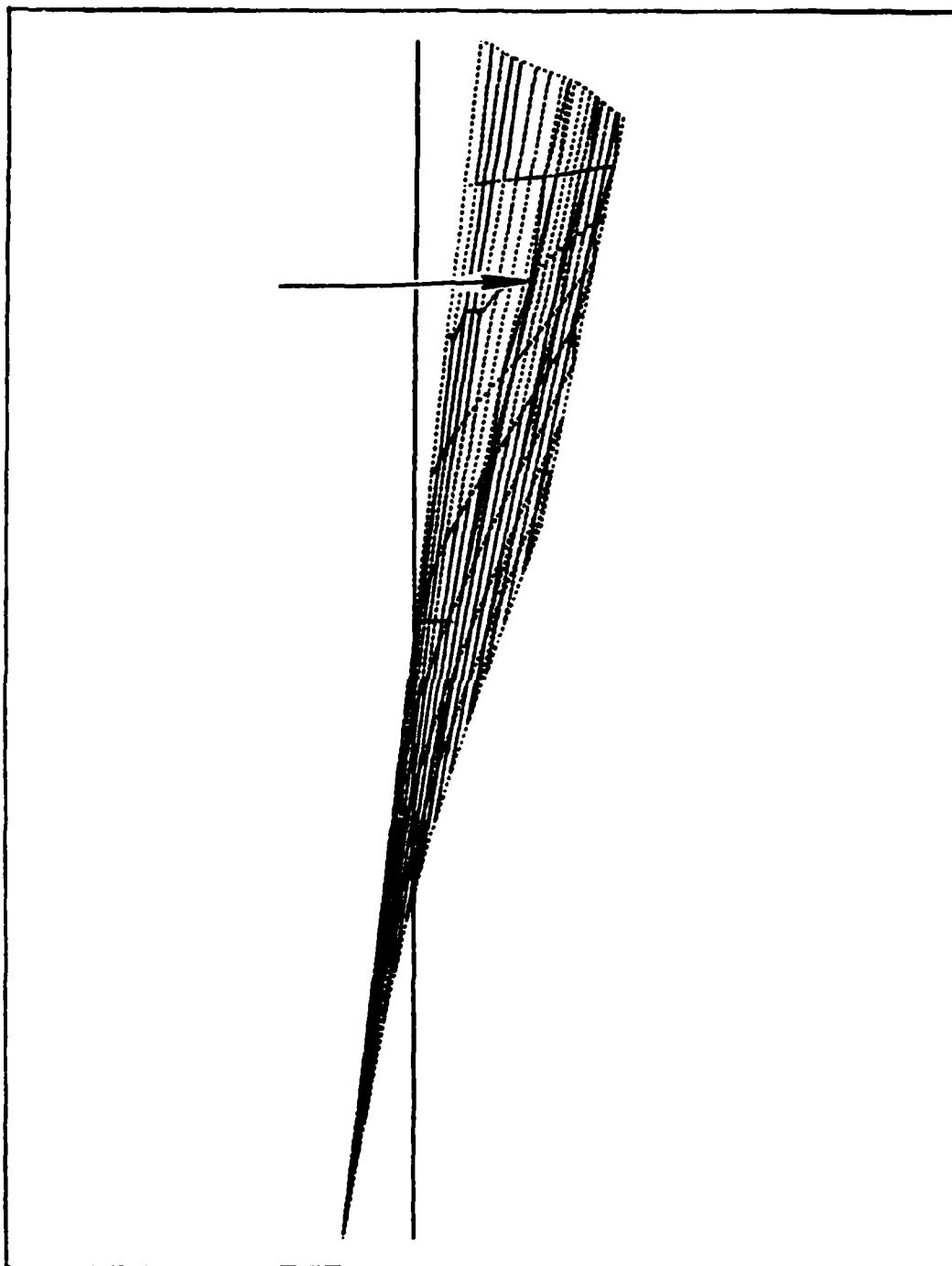


Figure G-7. Subcase 7 NASTRAN Analytical Deformation Due to
a 782 lb Load at GP 158

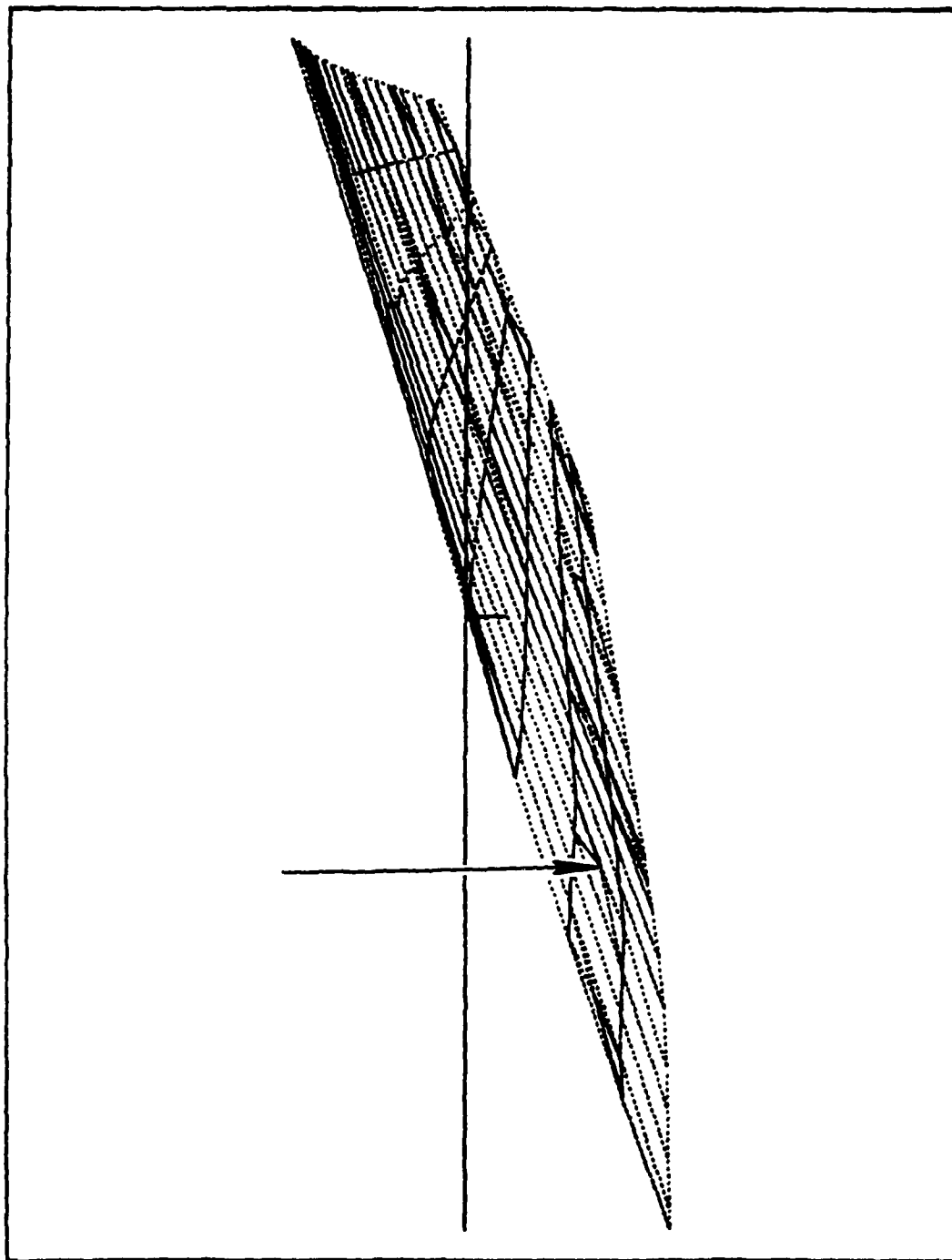


Figure C-8. Subcase 8 NASTRAN Analytical Deformation Due to
a 1182 lb Load at GP 160

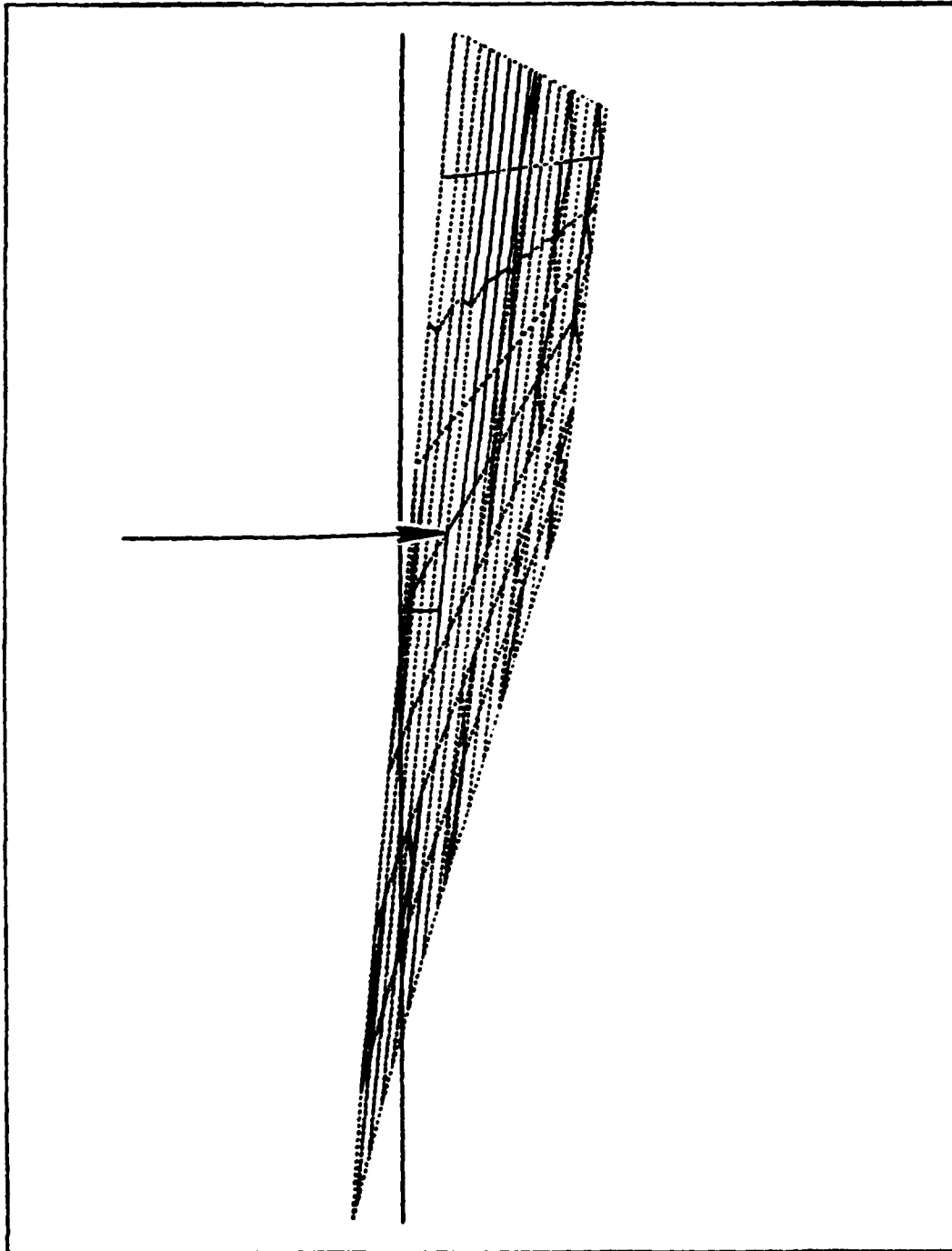


Figure G-9. Subcase 9 NASTRAN Analytical Deformation Due to
a 1182 lb Load at GP 104 .

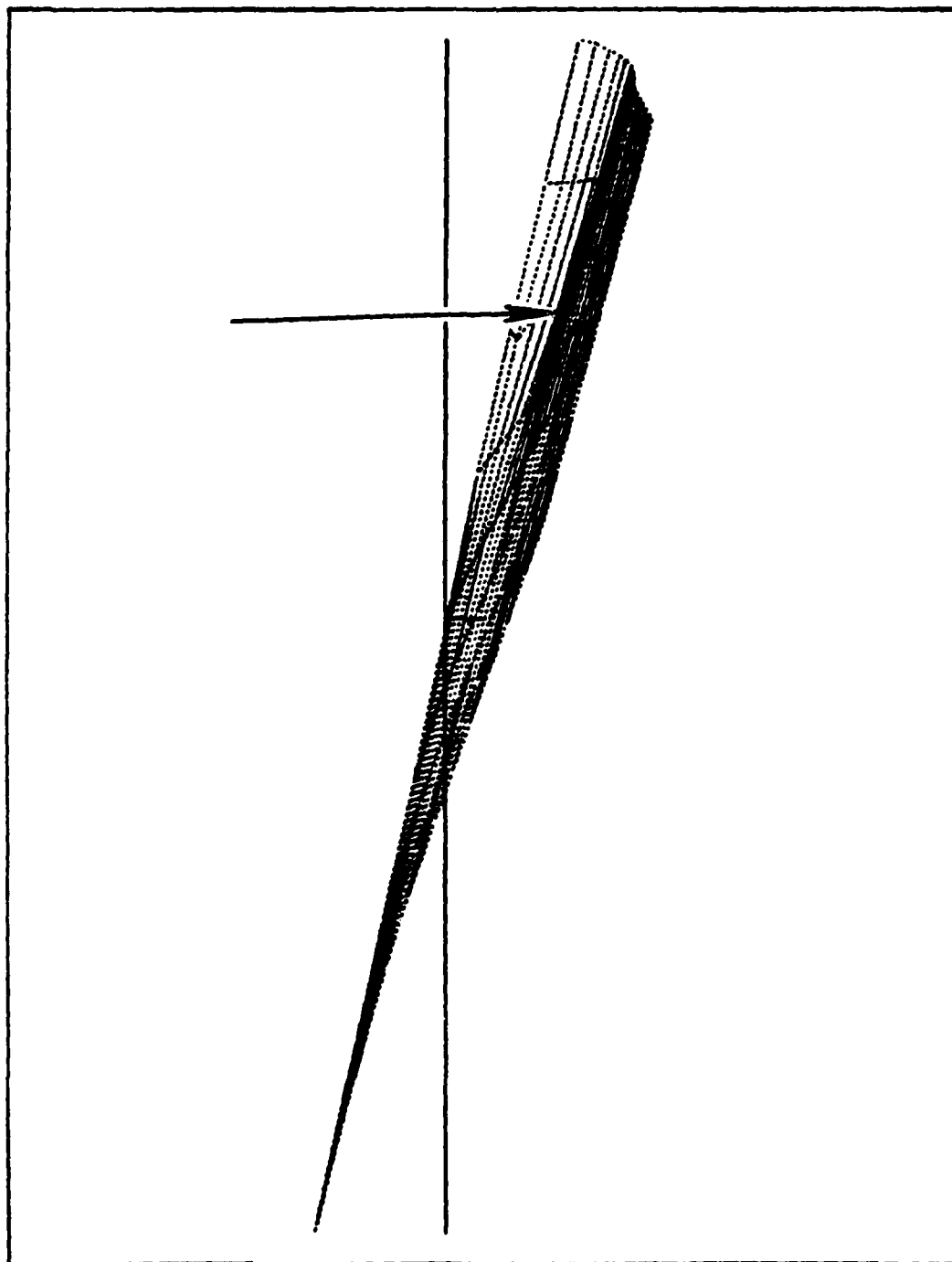


Figure G-10. Subcase 10 NASTRAN Analytical Deformation Due to
a 1182 lb Load at GP 106

VITA

Jack Orin Sawdy was born on 29 May 1951 in Louisville, Kentucky. He graduated from Valley High School in Louisville in 1969 and attended the University of Kentucky from which he received the degree of Bachelor of Science in Mechanical Engineering in December 1973. He received a commission in the USAF through the ROTC program. He entered active duty in March 1974. He served as a Landing Gear Project Engineer for Ogden Air Logistics Center, Hill AFB, Utah. In March 1978, he was reassigned as an Air Launched Cruise Missile Mechanical Systems Project Engineer for the 6510 Test Wing at Edwards AFB, California. Capt Sawdy was selected to attend the School of Engineering, beginning June 1980, at the Air Force Institute of Technology, Wright-Patterson AFB, Ohio to earn a Master's Degree in Aeronautical Engineering. His next assignment after graduation is with AFWAL, Wright-Patterson AFB, Ohio.

Permanent Address: 6603 Falling Star Drive
Louisville, Kentucky 40272

UNCLASSIFIED

SECURITY CLASSIFICATION OF THIS PAGE (When Data Entered)

REPORT DOCUMENTATION PAGE		READ INSTRUCTIONS BEFORE COMPLETING FORM
1. REPORT NUMBER AFIT/GAE/AA/81D-27	2. GOVT ACCESSION NO. AD-A111	3. RECIPIENT'S CATALOG NUMBER 100
4. TITLE (and Subtitle) INVESTIGATION OF A TWO-DIMENSIONAL MODEL FOR THE PREDICTION OF STATIC DISPLACEMENT FOR T-38 HORIZONTAL STABILATORS USING NASTRAN		5. TYPE OF REPORT & PERIOD COVERED AFIT THESIS
		6. PERFORMING ORG. REPORT NUMBER
7. AUTHOR(s) JACK O. SAWDY Capt USAF		8. CONTRACT OR GRANT NUMBER(s)
9. PERFORMING ORGANIZATION NAME AND ADDRESS Air Force Institute of Technology (AFIT/EN) Wright-Patterson AFB, Ohio 45433		10. PROGRAM ELEMENT, PROJECT, TASK AREA & WORK UNIT NUMBERS
11. CONTROLLING OFFICE NAME AND ADDRESS		12. REPORT DATE December 1981
		13. NUMBER OF PAGES 101
14. MONITORING AGENCY NAME & ADDRESS (if different from Controlling Office)		15. SECURITY CLASS. (of this report) Unclassified
		15a. DECLASSIFICATION DOWNGRADING SCHEDULE
16. DISTRIBUTION STATEMENT (of this Report) Approved for public release; distribution unlimited		
17. DISTRIBUTION STATEMENT (of the abstract entered in Block 20, if different from Report) Air Force Institute of Technology (ATC) 28 JAN 1982 Wright-Patterson AFB, OH 45433		
18. SUPPLEMENTARY NOTES Approved for public release; IAW AFR 190-17 Fredric C. Lynch, Major, USAF Director of Public Affairs <i>Fredric C. Lynch</i>		
19. KEY WORDS (Continue on reverse side if necessary and identify by block number) NASTRAN Finite Elements Static Analysis Error Value Function		
20. ABSTRACT (Continue on reverse side if necessary and identify by block number) This report documents the results of the experimental tests performed on a T-38 horizontal stabilator and the investigation of a two-dimensional finite element model for prediction of static displacement using NASA structural analysis (NASTRAN) computer program. The finite element model was used in previous and concurrent theses efforts with regard to T-38 flutter prediction via NASTRAN modal analysis methods. It will also be used in future analyses by a Using Air Force Agency for flutter prediction.		

DD FORM 1 JAN 73 1473 EDITION OF 1 NOV 65 IS OBSOLETE

UNCLASSIFIED

SECURITY CLASSIFICATION OF THIS PAGE (When Data Entered)

The experimental test set-up for the stabilator measured the displacements in the downward (water line) direction for ten load conditions with the displacements measured at twenty-five locations for each of the loading conditions. Precision load cells were used to measure the applied load and the resistance to rotation at the actuator arm. The boundary conditions of the tests represented an asymmetric loading condition for the T-38 assemblage.

The need for an improved two-dimensional finite element model was based on the results of previous flutter investigations using the same two-dimensional model. The model was to be used to analyze degradations in flutter speed due to repair. It was postulated that by optimizing the model characteristics for the static displacement cases that the improved model would better predict the flutter speed also.

The results of the experimental tests were compared with those developed using NASTRAN. Several of the model characteristics were altered and investigated as to their effect on the prediction of the static displacement. The analytical displacements were compared with those achieved experimentally.

Finally, development of an optimization procedure is presented, as well as its application to tuning the finite element model. The development of the optimization routine was based on current information for optimization techniques. A comparison is drawn between the error value used herein and current optimization theory.

FILMED
8